MATERIALS CHEMISTRY
FRONTIERS

REVIEW

View Article Online
View Journal | View Issue

Check for updates

Cite this: *Mater. Chem. Front.*, 2021, **5**, 4851

Sequential deposition enables high-performance nonfullerene organic solar cells

Miaomiao Li, [ab] Qi Wang,[ac] Junwei Liu,[a] Yanhou Geng [abc] and Long Ye *[abd]

Bulk-heterojunction active layers prepared by a blend casting (BC) method have been predominantly used for more than two decades in the construction of organic/polymer solar cells (OSCs) with high efficiencies and stability. Sequential deposition (SD) with donor and acceptor layers coated sequentially is a facile but effective strategy to fabricate efficient OSCs and holds great promise to address the drawbacks of bulk-heterojunctions. Compared with OSCs prepared by the BC method, SD processed OSCs can separately engineer different layers, realizing an ideal profile of vertical component distribution, which is favorable for charge generation, transport and collection. SD processed OSCs based on nonfullerene acceptors have progressed rapidly, with a striking power conversion efficiency (PCE) up to >18% achieved recently. In this review, we summarize recent advances in the optimization of SD processed OSCs with particular emphasis on the role of processing solvents and co-solvents, solvent additives and the third components. Moreover, we comprehensively discuss the impact of the SD method on device stability and provide an overview of the potential of the SD method in constructing large-area solar cell panels. Finally, we outline the existing challenges and prospects of the SD method in industrial production. We hope that this review can provide some inspiration for the performance improvement of SD processed OSCs and advance their commercial applications.

Received 16th March 2021,
Accepted 26th April 2021

DOI: 10.1039/d1qm00407g

rsc.li/frontiers-materials

Published on 27 April 2021. Downloaded by Yunnan University on 8/23/2025 11:05:38 AM.

[a] *School of Materials Science and Engineering, Tianjin University, Tianjin, 300072, China. E-mail: yelong@tju.edu.cn*
[b] *Tianjin Key Laboratory of Molecular Optoelectronic Science, Tianjin University, and Collaborative Innovation Center of Chemical Science and Engineering (Tianjin), Tianjin, 300072, China*
[c] *Joint School of National University of Singapore and Tianjin University, International Campus of Tianjin University, Binhai New City, Fuzhou, 350207, China*
[d] *State Key Laboratory of Luminescent Materials and Devices, South China University of Technology, Guangzhou, 510640, China*

Long Ye

Long Ye has been a Professor at the School of Materials Science & Engineering of Tianjin University since October 2019. He received his PhD degree from the Institute of Chemistry, Chinese Academy of Sciences (Adviser: Prof. Jianhui Hou) in 2015. From 2015 to 2019, he was a postdoctoral researcher and later promoted to research assistant professor in the same group headed by Prof. Harald Ade at the Department of Physics, North Carolina State University. His current interests include morphological and mechanical characterizations of semiconducting polymers and their blends in solar cells, diodes, and transistors, and polymer physics of conjugated polymers.

1. Introduction

In the past few decades, organic/polymer solar cells (OSCs) have drawn considerable attention due to their unique features such as low cost, light weight, and great potential in making large-area and flexible devices *via* a low-cost solution processing method.[1–14] Since the concept of a bulk heterojunction (BHJ) was proposed by Heeger *et al.* in 1995,[15] BHJs have been the dominant active layer structure for OSCs, due to the sufficient donor/acceptor interfacial area for exciton dissociation. With the development of photovoltaic materials, morphology control and device engineering, the power conversion efficiencies (PCEs) of BHJ OSCs have reached as high as 17–18% for single-junction and tandem devices.[16–35] In general, BHJ active layers are prepared from solvents composed of donor and acceptor materials by blend casting (BC), as schematically shown in Fig. 1. However, the formation process of BC active layers is exceedingly complicated, and the film morphology is highly dependent on processing conditions (such as donor : acceptor ratios, processing solvents, and post-treatments) and intrinsic properties of the material (such as solubility, aggregation behavior, and miscibility between the donor and acceptor).[36–45] Thus, it is extremely difficult for the BC method to precisely control and optimize the film microstructure, especially the distribution of the donor and acceptor components in the vertical direction of the film, thus leading to the risk of bimolecular recombination and poor charge extraction.[46–50]

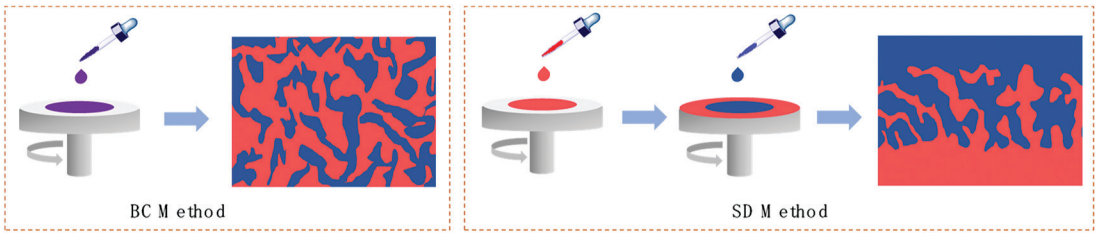

Fig. 1 Schematic diagrams of BC and SD processing methods and their corresponding film morphology.

Published on 27 April 2021. Downloaded by Yunnan University on 8/23/2025 11:05:38 AM.

Since charge carriers are transported and collected in the vertical direction within OSC devices, forming a preferred vertical phase distribution, *e.g.* donor-enrichment at the anode and acceptor-enrichment at the cathode, is beneficial to reducing charge recombination and promoting charge collection.[51–54] It is still a tough challenge for the BC method to form the preferred vertical phase distribution.

To achieve favorable film morphology with a suitable distribution of donor and acceptor components in the vertical direction, researchers have developed a sequential deposition (SD) method in which the donor solution and acceptor solution are coated sequentially to construct the active layer with a p–i–n like structure, where BHJ is formed in the middle and the donor and acceptor materials enrich at their desirable electrode sides (Fig. 1).[51,55–60] The p–i–n like morphology is beneficial for efficient exciton dissociation, and charge transport and extraction. In addition to the advantage in control of vertical phase distribution, the SD method is also superior to the BC method in the following aspects: (i) the donor layer and acceptor layer in the SD method are prepared separately, which allows precise manipulation and optimization of the microstructure of the donor and acceptor layers independently;[42,51,55,61,62] (ii) the SD method can help to overcome the limitations induced by intrinsic properties (crystallinity, miscibility, *etc.*) of the materials towards constructing more desired film morphology;[63] (iii) the SD method presents greater potential in fabricating devices with high thermal stability and photostability, which are key requirements in the commercialization of OSCs;[64–72] (iv) the SD method appears more suitable for large-area device fabrication, with high PCE retention when a small-area device is converted to its large-area counterpart.[65,73,74] Therefore, the SD method has become a facile and effective strategy to construct ideal film morphology, which is promising for the commercial application of OSCs. With enormous efforts on subtle manipulation of film morphology and device engineering, the SD processed OSCs have made great progress and their PCEs have exceeded 18% for a 0.04 cm^2 device[75] and 15% for a 1 cm^2 device.[74] To further increase the efficiency and advance the commercialization of OSCs, it is profoundly important and highly desired to derive the rationales of performance optimization and understand the effects of the SD method on the device stability and the performance of large-area devices.

In this review, we present an comprehensive overview of recent advances of SD solution processed OSCs. The molecular structures of the donors and acceptors in this review are shown in Fig. 2 and the photovoltaic metrics of SD processed devices are summarized in Tables 1–3. For clarity, we adopt "donor:-acceptor" and "donor/acceptor" to represent the material composition of BC and SD processed active layers, respectively. We start by detailing the morphology optimization strategies by evaluating the effects of processing solvents/co-solvents, solvent additives and the third component, which will help to provide valuable insights into the morphology control of SD processed active layers. In the next section, we summarize the influence of the SD method on the thermal stability and photostability of film morphology and device performance, followed by discussing the performance retention for SD processed OSCs from small-area laboratory-scale devices to large-area industrial-scale modules. Finally, we present the remaining challenges and the prospects of SD processed OSCs. We hope that this review can provide some enlightenment for the optimization of SD processed OSCs and help to accelerate their commercial applications.

2. Morphology optimization strategies for SD processed OSCs

In organic or polymer semiconductors, the exciton diffusion length is generally lower than 20 nm. Thereby, it is difficult for SD active layers with a flattened interface between the donor layer and the acceptor layer to gain efficient light absorption and exciton dissociation simultaneously, which leads to inferior J_{sc} and PCEs.[55,76–80] When the thicknesses of the donor layer and the acceptor layer are low (*e.g.*, ~20 nm), the devices present efficient exciton dissociation but poor light absorption. In contrast, the thick donor and acceptor layers (*e.g.*, 50–100 nm) result in inefficient exciton dissociation, due to the constraints of exciton diffusion length. Consequently, to achieve high efficiency, it is necessary for SD processed OSCs to construct p–i–n like active layers with suitable thickness of the donor and acceptor layers and sufficient intermixing between the two layers. In other words, the optimal SD processed films should possess sufficient film thickness and donor/acceptor interface in the bulk for efficient exciton generation and dissociation, as well as favorable vertical composition distribution for efficient charge collection. In addition, the ordered molecular packing and bicontinuous network structure are also of importance, which is constructive to charge transport. In this section, we summarize the morphology optimization strategies of the p–i–n like active layers, including solvent

 This journal is © The Royal Society of Chemistry and the Chinese Chemical Society 2021

Published on 27 April 2021. Downloaded by Yunnan University on 8/23/2025 11:05:38 AM.

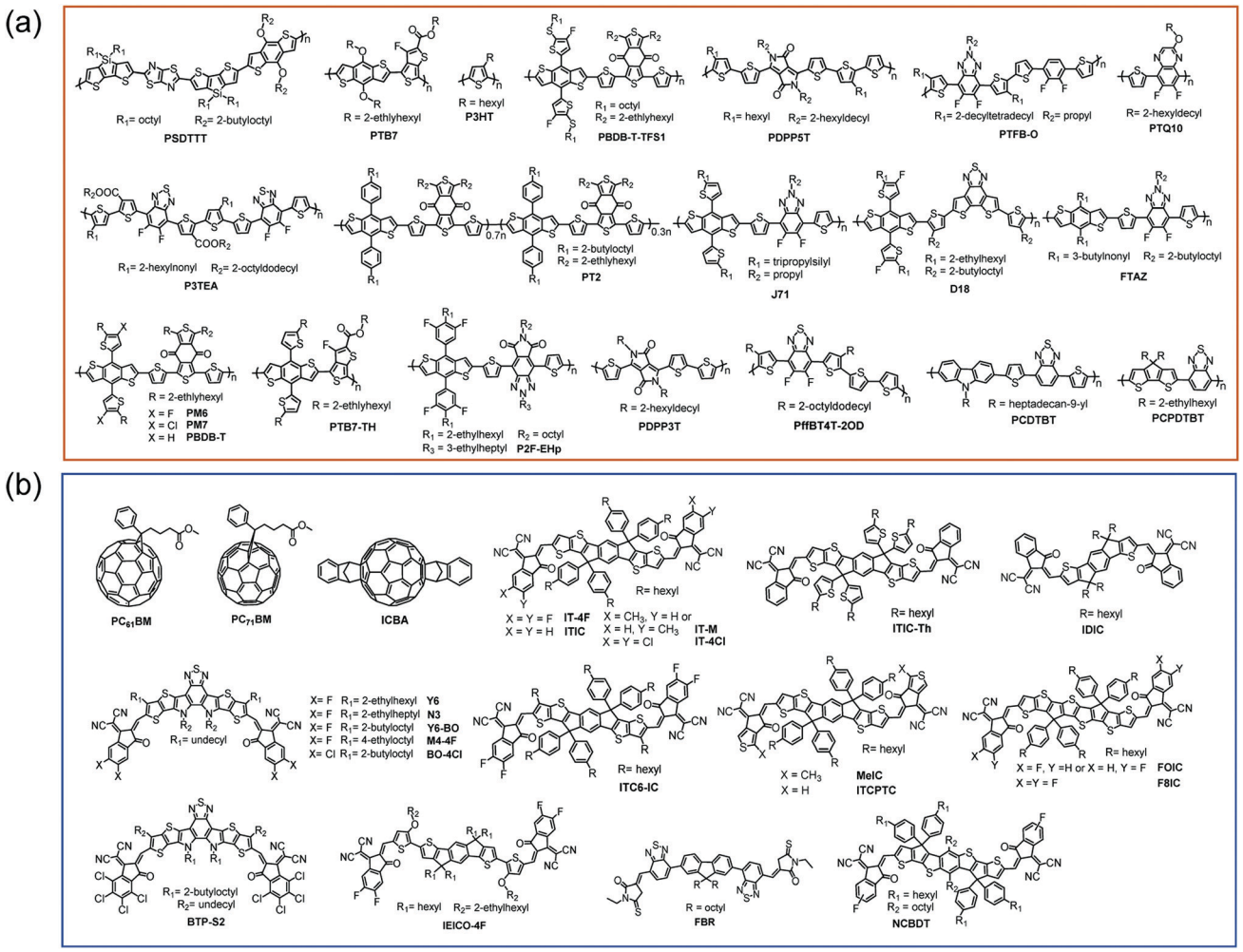

Fig. 2 The molecular structures of (a) donor and (b) acceptor materials involved in this review.

engineering to manipulate the lateral and vertical phase separation in the active layers, using high-boiling-point solvent additives to tune the molecular ordering, and introducing the third component to improve light absorption and modulate the film microstructure.

2.1 Solvent and co-solvent engineering

Optimizing solvents and co-solvents is an effective and facile way to modulate the interdiffusion between the donor layer and the acceptor layer and achieve ideal p–i–n like film morphology. For the SD method, the lower layer cannot be dissolved quickly and washed off completely by the upper layer casting, in order to achieve the desired morphology and good reproducibility. In the meantime, the efficient interdiffusion between the donor layer and the acceptor layer should be formed during the upper layer deposition. Therefore, it is crucial to screen suitable semi-orthogonal processing solvents and co-solvents, which can not only enable the formation of sufficient donor/acceptor interfaces but also avoid the dissolution and destruction of the lower layer.

To fabricate proper morphology *via* the SD method, in 2015, Schwartz *et al.* proposed to deposit the upper fullerene layer using the mixed solvents comprising a main solvent with high solubility for the fullerene acceptor and relatively low solubility for most polymer donors, and a co-solvent that can swell or wet the underlying polymer layer.[81] To simplify the solvent screening, the main solvent was fixed to 2-chlorophenol (2-CP) which can meet the solubility requirements. Aiming to achieve appropriate donor/acceptor interdiffusion, the Flory–Huggins interaction parameter (χ) between the fullerene processing solvent and the polymer donor should be manipulated into an optimal range by choosing a suitable co-solvent and altering the addition amount of the co-solvent. The calculated χ values between the polymer donors and toluene or isopropyl alcohol (IPA) are displayed in Fig. 3a. The lower χ value represents the stronger interaction between the solvent and the polymer donor, or the higher solubility of the polymer in the solvent. As expected, both PSDTTT and PTB7 exhibited much better solubility in toluene than IPA. The solubility of PTB7 is generally higher than that of PSDTTT, which is coincident with the lower χ values of PTB7 relative to those of PSDTTT for a given solvent.

Published on 27 April 2021. Downloaded by Yunnan University on 8/23/2025 11:05:38 AM.

Table 1 The photovoltaic parameters of OSC devices processed with different solvents

Active layer	Processing method	Solvent	Film thickness (nm)	V_{oc} (V)	J_{sc} (mA cm^{-2})	FF (%)	PCE (%)	Ref.
PSDTTT/$PC_{71}BM$	SD	CB/2-CP : toluene (35 : 65)	—	0.73	9.5	54	3.8	81
PSDTTT:$PC_{71}BM$	BC	CB	—	0.78	6.8	66	3.6	81
PTB7/$PC_{71}BM$	SD	CB/2-CP : 1-BuOH (50 : 50)	—	0.76	13.7	57	6.0	81
PTB7:$PC_{71}BM$	BC	CB : DIO (97 : 3)	—	0.74	13.3	57	5.9	81
P3HT/$PC_{61}BM$	SD	CB/2-CP : toluene (65 : 35)	—	0.50	6.4	45	1.4	81
		DCM	—	0.47	3.7	56	1.0	81
		DCM	—	0.63	7.7	64	3.1	81
PBDB-TFS1/IT-4F	SD	CB/THF	~50/~50	0.86	18.5	51	8.11	82
		CB/THF : *o*-DCB (95 : 5)	~50/~50	0.90	20.3	71	13.0	82
PBDB-TFS1:IT-4F	BC	CB	~100	0.87	19.9	68	11.8	82
PDPP5T/$PC_{71}BM$	SD	CF/toluene	—	0.58	0.53	31	0.1	83
		CF/*m*-xylene	—	0.58	2.04	43	0.5	83
		CF/*o*-xylene	—	0.57	10.0	56	3.2	83
		CF/TMB	—	0.57	15.1	61	5.3	83
PTFB-O/ITIC-Th	SD	CB/THF	~50/~50	0.910	17.5	74	11.8	85
		CB/CF	~50/~50	0.904	17.2	75	11.6	85
		CB/toluene	~50/~50	0.922	16.8	76	11.7	85
PTFB-O:ITIC-Th	BC	CB	~100	0.926	14.9	75	10.4	85
P3TEA/IT-4F	SD	TMB/CF	—	0.83	16.00	71	9.48	85
		TMB/THF	—	0.82	17.32	69	9.80	85
		TMB/toluene	—	0.83	16.15	70	9.38	85
		TMB/CB	—	0.84	15.42	74	9.55	85
		TMB/*o*-xylene	—	0.83	15.40	75	9.58	85
P3TEA:IT-4F	BC	TMB	—	0.82	15.41	69	8.76	85
PT2/Y6	SD	CB/CF	50/60	0.87	24.7	57.6	12.4	86
		CB/CF:DIO	50/60	0.83	26.7	74.4	16.5	86
PT2:Y6	BC	CB	110	0.83	26.3	68.9	15.0	86
FTAZ/IT-M	SD	TMB/2-MeTHF	—	0.959	15.7	55.5	8.9	87
		CB/2-MeTHF	—	0.940	17.4	59.3	10.7	87
		XY/2-MeTHF	—	0.958	17.3	61.7	10.7	87
		DMA/2-MeTHF	—	0.948	16.0	64.9	10.2	87
		LM/2-MeTHF	67/41	0.958	18.3	70.0	12.5	87
FTAZ:IT-M	BC	Toluene	—	0.968	17.8	68.1	12.0	87
D18/N3	SD	CF/CF	—	0.832	26.71	74.62	16.58	88
		CF/*n*-octane/CF	—	0.834	27.79	75.61	17.52	88
D18:N3	BC	CF	—	0.834	25.53	71.98	15.32	88
PM6/IT-4F	SD	CB/CB	—	0.90	19.18	70.24	12.13	89
		CB/CB : DIO (99 : 1)	—	0.86	20.98	75.90	13.70	89
		CB : DIO (99 : 1)/CB	—	0.90	19.15	70.27	12.11	89
PM6:IT-4F	BC	CB	—	0.90	19.16	69.79	12.04	89
		CB : DIO (99 : 1)	—	0.86	20.34	74.92	13.11	89
PM6/BO-4Cl	SD	CF/CF	50/50	0.836	26.1	74.2	16.2	90
		CF/CF : CN (99.75 : 0.25)	50/50	0.847	26.2	77.5	17.2	90
PM6:BO-4Cl	BC	CF : CN (99.75 : 0.25)	110	0.841	25.8	75.6	16.4	90
PM6/Y6	SD	CB/CF	61/48	0.85	26.6	65.5	14.8	91
		CB/CF : DIO (99.5 : 0.5)	—	0.82	26.3	76.3	16.5	91
PM6:Y6	BC	CF : CN (99.5 : 0.5)	—	0.85	25.3	73.5	15.8	91
P2F-EHp/M4-4F	SD	CF	—	0.86	21.44	64.45	11.85	92
		CF/CF : DBE (98 : 2)	—	0.83	25.56	67.14	14.21	92
P2F-EHp:M4-4F	BC	CF	—	0.88	23.86	55.47	11.72	92
		CF : DBE (99.9 : 0.1)	—	0.84	23.66	64.05	12.77	92

The χ value between 1.4 and 2 was estimated as the optimal range to make the acceptor solution sufficiently swell the polymer layer without disrupting the ordered polymer regions. For polymer PSDTTT that is completely insoluble in 2-CP with high χ above 2.5 at room temperature, a good solvent for PSDTTT, *i.e.* toluene, was selected as the co-solvent to adjust the χ of the mixed solvent to the desired range. When the volume ratio of 2-CP and toluene was 65 : 35, the χ value of the mixed solvent was decreased to about 1.5. With 2-CP : toluene (65 : 35) as the processing solvent for $PC_{61}BM$, the PSDTTT based SD solar cells obtained a PCE of 3.8%, which was slightly higher than that of the BC processed devices (3.6%). For polymer PTB7 that is slightly soluble in 2-CP with a relatively low χ value below 1, a poor co-solvent for PTB7, such as IPA, was required to increase the χ value of the solvent for fullerene deposition. As expected, the processing solvent of 2-CP : IPA (70 : 30) with χ of ~1.4 for fullerene deposition enabled the formation of the BHJ network and afforded a good device efficiency of 4.3%. To further prevent the dissolution of PTB7 during fullerene casting, the co-solvent IPA was replaced with 1-butanol (1-BuOH) that possesses higher χ with the polymer. The PCE of the PTB7 based SD device processed with 2-CP : 1-BuOH (50 : 50) was further increased to 6.0%, comparable to that of the blend-cast device (5.9%). Different from PSDTTT and PTB7 which are

 This journal is © The Royal Society of Chemistry and the Chinese Chemical Society 2021

Published on 27 April 2021. Downloaded by Yunnan University on 8/23/2025 11:05:38 AM.

Table 2 The photovoltaic parameters of binary and ternary OSC devices

Active layer	Processing method	Film thickness (nm)	V_{oc} (V)	J_{sc} (mA cm^{-2})	FF (%)	PCE (%)	Ref.
PBDB-T:IT-M	BC	100	0.918	15.24	69.30	10.04	93
PBDB-T:FOIC	BC	100	0.721	22.64	63.46	10.45	93
PBDB-T:IT-M/PBDB-T:FOIC	SD	15/100	0.751	24.66	63.57	11.91	93
PDPP3T:$PC_{71}BM$	BC	80	0.64	14.40	67.05	6.39	63
FTAZ:$PC_{71}BM$	BC	75	0.75	10.39	73.82	5.86	63
PDPP3T:FTAZ:$PC_{71}BM$	BC	90	0.63	12.01	65.29	5.09	63
PDPP3T:$PC_{71}BM$/FTAZ:$PC_{71}BM$	SD	—	0.69	15.67	61.86	6.73	63
PM6:BO-4Cl	BC	115	0.842	26.36	74.92	16.64	75
PM6/BO-4Cl	SD	—	0.846	26.81	75.40	17.11	75
PM6:BTP-S2	BC	115	0.941	21.84	72.68	14.95	75
PM6/BTP-S2	SD	—	0.942	21.98	72.57	15.04	75
PM6:BO-4Cl:BTP-S2	BC	115	0.856	27.11	77.98	18.03	75
PM6/BO-4Cl:BTP-S2	SD	—	0.861	27.14	78.04	18.16	75
PM6:IT-4F	BC	—	0.85	20.76	74.04	13.04	94
PM6/IT-4F	SD	—	0.85	20.81	74.13	13.19	94
PM6:ICBA	BC	—	1.12	7.08	49.74	3.94	94
PM6/ICBA	SD	—	1.11	7.19	49.74	3.98	94
PM6:IT-4F:ICBA	BC	—	0.87	20.96	75.45	13.73	94
PM6/IT-4F:ICBA	SD	—	0.88	21.25	76.55	14.25	94
PM6:IT-4F	BC	100	0.86	20.4	74.0	13.0	95
PM6:IT-4F:F8IC	BC	115	0.80	24.4	70.7	13.8	95
PM6/IT-4F:F8IC	SD	100/25	0.79	25.6	69.8	14.2	95
PM6:N3:$PC_{71}BM$	BC	—	0.840	25.69	76.2	16.44	96
PM6/N3:$PC_{71}BM$	SD	50/49	0.841	26.49	78.2	17.42	96
PffBT4T-2OD:IEICO-4F	BC	110	0.72	20.8	69.3	10.4	97
PffBT4T-2OD/IEICO-4F	SD	60/50	0.71	20.9	71.4	10.6	97
PffBT4T-2OD:FBR	BC	110	1.08	11.8	63.3	8.1	97
PffBT4T-2OD/FBR	SD	60/50	1.08	12.7	66.1	9.1	97
PffBT4T-2OD:IEICO-4F:FBR	BC	110	0.75	21.5	65.4	10.5	97
PffBT4T-2OD/IEICO-4F:FBR	SD	60/50	0.74	22.4	68.3	11.3	97

Table 3 The photovoltaic parameters of OSC devices under a stability test

Active layer	Processing method	Stability test	Film thickness (nm)	$V_{oc}{}^{d}$ (V)	$J_{sc}{}^{d}$ (mA cm^{-2})	FF^{d} (%)	PCE^{d} (%)	PCE^{e}/PCE^{d} (%)	Ref.
PCDTBT/$PC_{71}BM$	SD	Heating at 80 °C for 10 days	—	0.82	9.87	62	5.03	97	69
PCDTBT:$PC_{71}BM$	BC		—	0.53	9.00	31	4.00	38	69
PTB7-TH/$PC_{71}BM$	SD	Heating at 130 °C for 120 min	80/50	0.81	16.6	62.7	8.5	60	64
PTB7-TH:$PC_{71}BM^{a}$	SD		80/50	0.81	16.5	61.9	8.3	~100	64
PTB7-TH/$PC_{71}BM$	BC		100	0.76	15.8	68.8	8.3	43	64
PTB7-TH:$PC_{71}BM^{a}$	BC		100	0.76	13.8	59.2	6.2	76	64
PTB7/$PC_{71}BM$	SD	Heating at 140 °C for 10 days	—	0.768	14.8	65.4	7.43	96	68
PTB7:$PC_{71}BM$	BC		80/10	0.760	14.7	64.3	7.17	78	68
PCPDTBT/$PC_{71}BM^{b}$	SD	Heating at 80 °C for 12 days	—	0.63	10.16	48	3.06	~70	67
PCPDTBT/$PC_{71}BM^{c}$	SD		—	0.63	10.66	49.9	3.36	~70	67
PCPDTBT:$PC_{71}BM$	BC		—	0.62	11.88	52.5	3.87	~40	67
PffBT4T-2OD/$PC_{71}BM$	SD	Illumination (100 mW cm^{-2})	90/30	0.76	16.5	75	9.12	83	65
PffBT4T-2OD: $PC_{71}BM$	BC	for 500 h	120	0.76	16.8	73	9.04	72	65
J71/ITC6-IC	SD	Illumination (100 mW cm^{-2})	—	0.968	16.85	70.1	11.47	~85	71
J71:ITC6-IC	BC	for 500 h	—	0.950	16.15	67.8	10.41	~68	71

[a] The films were pre-annealed at 100 °C for 20 min. [b] The polymer layer was processed with CN additive. [c] The polymer layer was processed with DIO additive. [d] Photovoltaic parameters of the devices before long-term thermal annealing or illumination. [e] PCE values of the devices after long-term thermal annealing or illumination.

fairly amorphous, P3HT is a semi-crystalline polymer. As shown in Fig. 3a, the χ value between IPA and the P3HT film was dependent on the P3HT casting solvents and post-treatments. The P3HT films processed with high-boiling-point solvent *o*-dichlorobenzene (*o*-DCB) or thermally annealed showed much higher χ values with IPA in comparison to the film prepared from chloroform without any post-treatment, probably because the highly ordered polymer film is more impervious for the infiltration of the solvent. Like PSDTTT, P3HT cannot dissolve in 2-CP, and hence toluene was chosen as the co-solvent to pair with 2-CP. The PCE of the P3HT:$PC_{61}BM$ based SD device with 2-CP : toluene (35 : 65) as the processing solvent for $PC_{61}BM$ deposition (1.4%) was superior to that of the SD device made by the commonly-used dichloromethane (DCM) (1.0%), and it increased to 3.1% upon thermal annealing, which was conducted to further drive fullerene into the ordered polymer layer. This study offers selection rules of the fullerene solvents for various underlying polymers by elevating the χ

Published on 27 April 2021. Downloaded by Yunnan University on 8/23/2025 11:05:38 AM.

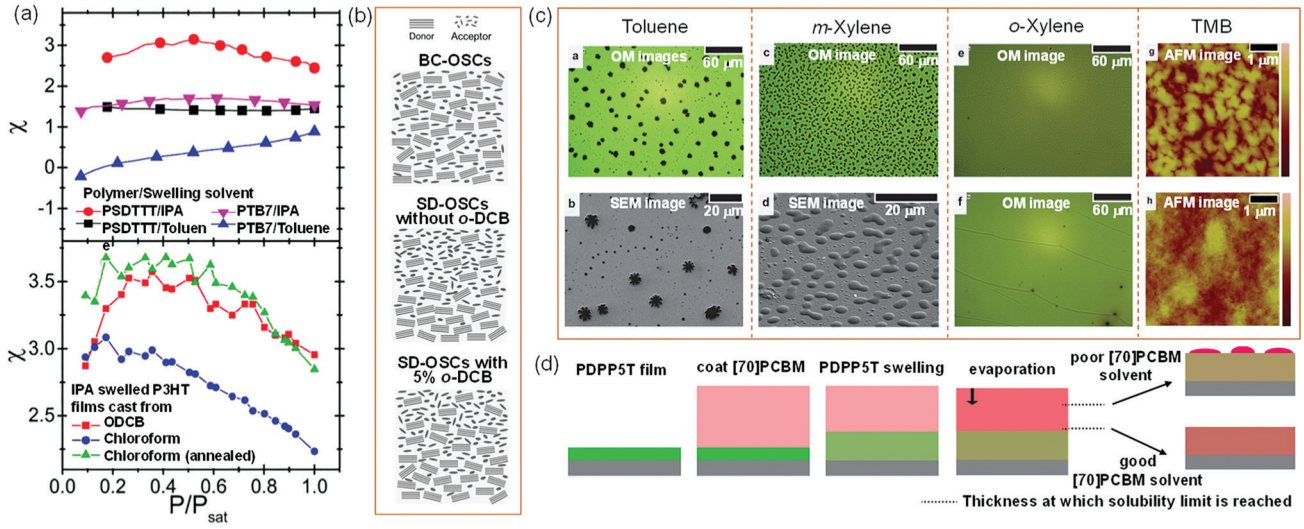

Fig. 3 (a) The χ values *versus* the ratios of swelling solvent (toluene or IPA) pressure and its saturation pressure (P/P_{sat}) for PTB7, PSDTTT films and P3HT films exposed to the swelling solvent vapor. The pressures of toluene and IPA were measured by ellipsometry. The P_{sat} values are 29 and 45 torr for toluene and isopropanol, respectively. Reproduced with permission.[81] Copyright 2015, Wiley. (b) Schematic illustration of the morphology of BC processed PBDB-TFS1:IT-4F film and SD processed PBDB-TFS1/IT-4F films without and with *o*-DCB. Reproduced with permission.[82] Copyright 2018, Wiley. (c) OM, SEM and AFM height images (height scale 40 nm) of SD processed PDPP5T/$PC_{71}BM$ blend films, using toluene, *m*-xylene, *o*-xylene and TMB as second-layer solvents. (d) Schematic illustration of the SD processing for PDPP5T/$PC_{71}BM$ blend films with different solvents for $PC_{71}BM$. Reproduced with permission.[83] Copyright 2015, Wiley.

parameter of the solvent–polymer layer pairs, which enables rational morphology control towards the desirable p–i–n like morphology *via* the SD method.

In 2018, Hou *et al.* utilized a mixed solvent strategy to deposit the nonfullerene acceptor upper layer, using PBDB-TFS1 as a donor and IT-4F as an acceptor due to their significant difference in solubility.[82] The polymer donor PBDB-TFS1 presents poor solubility in common organic solvents at room temperature but is soluble in *o*-DCB at increased temperature. Acceptor IT-4F dissolves well in common organic solvents, such as tetrahydrofuran (THF), but in which PBDB-TFS1 presents a very low solubility. To construct an ideal p–i–n like morphology, the main solvent of the upper acceptor layer should have high solubility for the acceptor material but low solubility for the underlying polymer donor material, and the co-solvent should have high boiling point and be able to swell and wet the polymer layer. Based on the solvent selection rules, THF and *o*-DCB were selected as the main solvent and co-solvent, respectively. The main solvent THF will be evaporated rapidly, and *o*-DCB with high boiling point will be concentrated and hence drive IT-4F to penetrate into the PBDB-TFS1 film. As such, the interdiffusion between PBDB-TFS1 and IT-4F and the device performance can be effectively optimized by tuning the fractions of *o*-DCB in the THF:*o*-DCB mixture. Additionally, the surface energy was measured by the contact angle method to evaluate the vertical distribution of IT-4F in the blend films with different processing methods. All the blend films presented surface energy between that of neat PBDB-TFS1 film (29.3 mJ m^{-2}) and that of IT-4F film (30.5 mJ m^{-2}), and the surface energy values of the SD blend films without *o*-DCB (30.2 mJ m^{-2}) and with 5% *o*-DCB (29.8 mJ m^{-2}) were significantly higher than that of the BC blend film (19.5 mJ m^{-2}), suggesting the higher content of the acceptor component on the film surface. The decreased energy surface upon addition of 5% *o*-DCB into the acceptor solution indicates the better diffusion between IT-4F and PBDBTFS1. The X-ray photoelectron spectroscopy (XPS) results also show that the acceptor in the SD films was more enriched on the top surface compared to the BC film, and the addition of *o*-DCB promoted the acceptor to diffuse downward into the underlying polymer layer, as schematically illustrated in Fig. 3b. Owing to the suitable film morphology with sufficient donor/acceptor interface and favorable vertical component distribution, the SD processed device with 5% *o*-DCB exhibited a PCE of 13.0%, which was higher than those of the BC processed devices (11.8%) and the SD processed devices without *o*-DCB (8.11%).

As mentioned above, the p–i–n like morphology of the SD processed active layer is largely determined by the properties of the upper layer solvent. In addition to the ability to swell the underlying polymer, do other parameters of the upper-layer solvent also influence the film morphology and device performance? To answer this question, Janssen and co-workers varied the processing solvents of the upper $PC_{71}BM$ layer to fabricate SD solar cells with poly(diketopyrrolopyrrole-*alt*-quinquethiophene) (PDPP5T) as the bottom donor layer.[83] The tested non-halogenated processing solvents like toluene, *m*-xylene, *o*-xylene and 1,2,4-trimethylbenzene (TMB) can swell the PDPP5T film similarly, but the corresponding devices displayed greatly different performance with PCE of 0.1%, 0.5%, 3.2% and 5.3%, respectively. From the film morphology characterized by optical microscopy (OM) and scanning electron microscopy (SEM) and atomic force microscopy (AFM) (see Fig. 3c), different from the *o*-xylene and

 This journal is © The Royal Society of Chemistry and the Chinese Chemical Society 2021

Published on 27 April 2021. Downloaded by Yunnan University on 8/23/2025 11:05:38 AM.

TMB processed films with a relatively uniform surface, the films with toluene and *m*-xylene as the processing solvent of $PC_{71}BM$ showed micron-sized dendritic crystallites and droplet-like domains on the surface, which can explain the poor device performance. In addition, the OM images show that the film between the droplets looks in the toluene and *m*-xylene processed active layers greener relative to the *o*-xylene and TMB processed active layers, suggesting a lower content of $PC_{71}BM$ in PDPP5T film. For the *o*-xylene and TMB processed films with similar uniform OM images, the difference in film microstructure was observed by AFM. A homogeneous morphology was observed for the TMB processed film, whereas the *o*-xylene processed film presented an inhomogeneous surface and quasi-bilayer structure, resulting from aggregation of $PC_{71}BM$ on top of the polymer-rich film. After excluding the effects of the melting point of these processing solvents, they ascribed the various film morphologies to the different solubility of the $PC_{71}BM$ in these solvents. As schematically illustrated in Fig. 3d, during casting of the upper layer, $PC_{71}BM$ solution diffuses into the polymer layer, and reaches the solubility limit at some moment as the solvent evaporates. At this point in time, for the processing solvent with low solubility, $PC_{71}BM$ is precipitated from the solution that is left on top of the polymer layer, resulting in poor donor/acceptor intermixing morphology with large dendritic crystallites or droplet-like domains on the top. By contrast, the solvent with high solubility allows the infiltration of $PC_{71}BM$ in the underlying polymer film more sufficiently, yielding a better interdiffusion between PDPP5T and $PC_{71}BM$. The measured solubility of the four processing solvents follows the order of toluene (50 mg mL^{-1}) < *m*-xylene (101 mg mL^{-1}) < *o*-xylene (229 mg mL^{-1}), TMB (224 mg mL^{-1}). Thus, better film morphology and higher PCEs were obtained by the devices processed from *o*-xylene and TMB. Given that the solubility of $PC_{71}BM$ in *o*-xylene and TMB is so high that it cannot be measured accurately, the difference between the devices made from *o*-xylene and TMB might be caused by the higher solubility of $PC_{71}BM$ in TMB than that in *o*-xylene, as hinted from the report that the solubility of C_{60} in TMB (17.9 mg mL^{-1}) is more than twice that in *o*-xylene (8.7 mg mL^{-1}).[84]

For some crystalline or semi-crystalline underlying polymer donors that are more impervious to the solvent infiltration, the ideal film morphology can be obtained by depositing the overlying acceptor layer from some non-orthogonal solvents or the same solvent with the polymer. For example, Yan *et al.* used the conjugated polymer donors PTFB-O and P3TEA with high crystallinity to construct a p–i–n like active layer *via* the SD method.[85] These polymer donors can be processed into solid films by high-temperature solution, but the resulting films cannot be dissolved at room temperature. This property allows for the acceptor to be processed on the top of the polymer layer from various non-orthogonal solvents. All the PTFB-O/ITIC-Th based SD devices in which the donor was dissolved in TMB and the acceptor upper layer was processed from THF, chloroform (CF) and toluene, afforded high PCE exceeding 11%, comparable to their BC counterparts with a PCE of 10.4%. Similarly, the P3TEA/IT-4F based SD devices with different processing solvents (including CF, THF, toluene, chlorobenzene (CB) and *o*-xylene with largely different boiling points) for the overlying acceptor IT-4F also exhibited superior performance (PCE over 9%) in comparison to the BC devices with TMB as the processing solvent (PCE = 8.76%). Recently, Sun *et al.* developed a polymer donor PT2 that can form well-defined fibril morphology, and processed this polymer with CB as the solvent followed by depositing acceptor Y6 with CF as the casting solvent.[86] For the SD processing, the CF solution of Y6 swelled the underlying PT2 layer and diffused into the polymer fibril mesh to form a p–i–n like film morphology as schematically illustrated in Fig. 4a, and the morphology was further optimized by 1,8-diiodooctane (DIO) solvent additive and thermal annealing (TA) treatment. As a result, a high PCE of 16.5% was achieved for the SD processed devices, outperforming the BC devices. In addition, due to the robust film morphology, the performance of SD devices was insensitive to the polymer batches with different molecular weights (M_n = 45, 57 and 91 kg mol^{-1}). Min *et al.* used the donor polymers (PTQ10 and J71) and the non-fullerene acceptors (IDIC, ITC6-IC, MeIC, ITCPTC and ITIC) to fabricate solar cells *via* the SD method using a single processing solvent (CF) for both donor and acceptor layers.[73] Owing to the enhanced optical absorption and appropriate morphology, the SD processed devices exhibited comparable or even higher PCEs relative to the corresponding BC devices.

In addition to the solvents of the upper layer, the solvents of the lower layer also influence the morphology of SD processed blend films. To modulate phase separation and optimize the photovoltaic performance of the SD blend films, Ye and co-workers used different processing solvents like CB, *o*-xylene, 1,2,4-trimethylbenzene (TMB), 2,6-dimethylanisole (DMA) and (*R*)-(+)-limonene (LM) to deposit bottom FTAZ layer.[87] The acceptor IT-M layer was sequentially cast with 2-methyltetrahydrofuran as processing solvent. The OSC devices with various processing solvents for the FTAZ layer displayed distinct photovoltaic performance. The TMB processed devices obtained the lowest PCE of 8.9%; the CB, XY and DMA processed devices showed moderate performance with the maximum PCEs of 10.7%, 10.7% and 10.2%, respectively; the highest PCE of 12.5% was achieved for the devices with LM as the casting solvent for FTAZ, which was superior to the best-performing device prepared by the BC method with a PCE of 11.9%. From the resonant soft X-ray scattering (RSoXS) results (Fig. 4b and c), domain spacing (or long period) of these SD blend films were strongly dependent on the processing solvents for FTAZ. The LM processed film gave the largest domain spacing of ~35 nm, which was also larger than that of the blend casting film (~20 nm). Besides, applying LM as the processing solvent for FTAZ enabled the enhancement of the molecular ordering for the weakly crystalline polymer. Owing to the suitable morphology with relatively large phase separation and high polymer crystallinity, the SD devices with LM as the solvent for FTAZ afforded the best photovoltaic performance. To obtain more insight into the difference in the morphology of the SD processed blend films, the interaction between polymer FTAZ and the various processing solvents was evaluated by calculating the volume normalized χ parameter between FTAZ

Published on 27 April 2021. Downloaded by Yunnan University on 8/23/2025 11:05:38 AM.

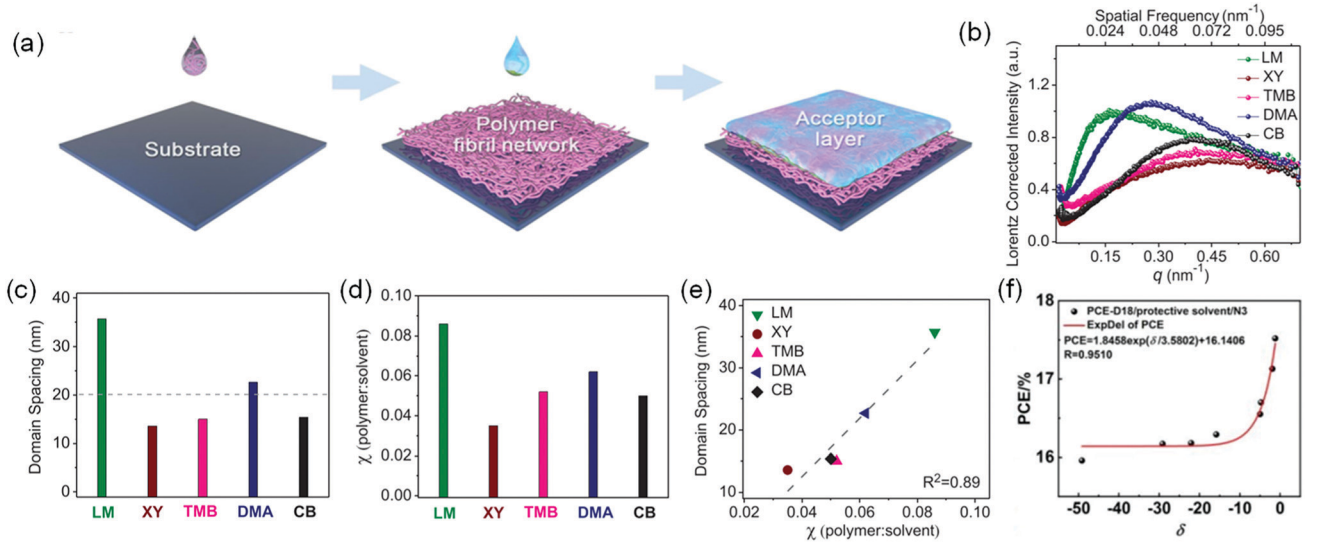

Fig. 4 (a) Schematic illustration of the SD deposition procedure of the PT2/Y6 blend. Reproduced with permission.[86] Copyright 2020, Springer Nature. (b) Lorentz-corrected RSoXS profiles of SD processed FTAZ/IT-M films with various solvents. The top axis of spatial frequency (s) can be transformed into momentum transfer with $q = 2\pi s$. (c) Long period of SD processed FTAZ/IT-M films with different solvents for FTAZ. (d) Estimated χ parameter between FTAZ and the processing solvent. (e) Domain spacing of FTAZ/IT-M films as a function of χ parameter between FTAZ and the processing solvent. The dashed line is a linear fit to the data. Reproduced with permission.[87] Copyright 2019, Wiley. (f) Relationship between δ of the protective solvent and PCE of SD processed D18/N3 devices. Reproduced with permission.[88] Copyright 2021, The Royal Society of Chemistry.

and the solvent (Fig. 4d). They found that there was an almost linear relationship between the polymer:solvent interaction parameter χ and the domain spacing of the SD blend film, as shown in Fig. 4e. For the LM processed blend film with the largest domain spacing, the χ value between the polymer and the solvent LM was the highest. This observation suggests that the χ parameter can serve as a useful tool to guide the selection of processing solvent and the manipulation of phase separation for SD devices.

Recently, Huang and co-workers reported a new strategy to fabricate high-efficiency SD OSCs by casting non-aromatic and non-halogenated solvents (like alcohol, alkane, ether, *etc.*) before the upper acceptor layer deposition to protect the lower polymer layer from destruction.[88] The protective effect of these solvents on the underlying layer was closely related to the two properties of the solvents, *i.e.* spreading coefficient (S) and saturated vapor pressure (P). The good protective solvents need to have a high spreading coefficient to ensure good spreading on the underlying polymer film, and relatively low saturated vapor pressure (P) so that the solvent molecules do not volatilize completely before the deposition of the acceptor solution. To evaluate the protective effect quantitatively, a new parameter protective factor (δ) was proposed by combining S and P with an expression as $\delta = S \log P$. It was observed that there was an exponential relationship between δ of the protective solvent and PCE of the SD processed D18/N3 devices (Fig. 4f). Clearly, when *n*-octane with δ parameter close to 0 was used as the protective solvent, the device delivered the highest PCE of 17.52%, which was superior to those of the SD devices with other protective solvents, as well as the SD devices without any protective solvent and the BC processed device. Other photovoltaic donor:acceptor systems like PM6/N3, PM6/Y6, PM7/Y6, PM6/IT-4F, PM6/IT-4Cl, PBDB-T/ITIC, PTB7-Th/PC71BM and P3HT/$PC_{71}BM$ exhibited similar relationship between δ parameter and device efficiency, yielding a higher device efficiency when the δ parameter was closer to 0. This work provides a new strategy to construct high-efficiency SD solar cells, which shows great potential as a universal strategy.

Overall, the processing solvents for the top layer and the bottom layer both significantly affect the film morphology. The suitable processing solvent enables the upper layer molecules to sufficiently permeate into the underlying layer and avoids destroying the underlying polymer layer. The permeation of the top layer solution into the bottom film largely depends on the properties of the semi-orthogonal solvents, such as the solubility for top and bottom layer materials and the interactions between the solvent and the photovoltaic materials. Besides, the high-efficiency SD blend films can also be obtained by introducing non-aromatic and nonhalogenated solvents as protective agents, or using non-orthogonal solvents to coat the upper layer for the underlying polymers that have high crystallinity. In these SD deposited active layers, the individual layer thicknesses of the donor and acceptor are critical to the performance, given the small, around 10 or a few dozens of nm, maximum, diffusion excitation lengths of donors and acceptors used in most efficient OSC devices. It is thus necessary to be cautious in fully exploring the thickness effect.

2.2 Incorporation of solvent additive

Due to their high boiling point and selective solubility, solvent additives, such as 1,8-diiodooctane (DIO), chloronaphthalene (CN), diphenyl ether (DPE) and *N*-methylpyrrolidone (NMP),

 This journal is © The Royal Society of Chemistry and the Chinese Chemical Society 2021

Published on 27 April 2021. Downloaded by Yunnan University on 8/23/2025 11:05:38 AM.

can be incorporated to improve molecular ordering, and adjust the phase separation of both SD and BC processed blend films. For the SD method, the high-boiling-point solvent additives can also be added to a certain layer solution, which enables selective optimization of donor or acceptor microstructure and precise control of the film morphology.

To explore the effect of the high-boiling-point additive DIO on the morphology and photovoltaic performance of the SD processed blend, Chen *et al.* fabricate PM6/IT-4F based SD OSCs without DIO (PM6/IT-4F), with DIO in PM6 solution (PM6(DIO)/IT-4F) and with DIO in IT-4F solution (PM6/IT-4F(DIO)), as well as the BC processed OSCs (PM6:IT-4F) without and with DIO (PM6:IT-4F:DIO) for comparison.[89] Among these devices, the SD processed device with DIO in IT-4F solution achieved the best performance with a PCE of 13.70%. The efficiencies of the BC (12.04%) and SD (12.13%) processed devices without DIO and the SD device with DIO in PM6 solution (12.11%) were similar, and all inferior to those of the PM6:IT-4F:DIO based BC device (13.11%) and the PM6/IT-4F(DIO) based SD device (13.70%). Obviously, for the SD method, the incorporation of DIO in the IT-4F solution resulted in much improved photovoltaic performance, whereas the efficiency remained unchanged when DIO was added into the PM6 solution. These results imply that solvent additive DIO may have a great impact on the microstructure of IT-4F instead of PM6. To further probe the effects of DIO, the morphology and molecular packing for the SD and BC processed blend films and the neat films of PM6 and IT-4F without and with DIO were studied by AFM and GIWAXS (Fig. 5a and b). Both SD and BC processed blend films without DIO showed small phase separation and smooth surfaces with root mean square roughness (R_q) of 2.20 and 1.95 nm. After the addition of DIO, the BC processed blend film (PM6:IT-4F:DIO) exhibited more pronounced phase separation with the R_q value increasing to 2.50 nm, which was responsible for the improved device performance. The R_q of the IT-4F neat film with DIO (marked by IT-4F:DIO) was sharply increased from 0.71 nm for the IT-4F neat film without DIO (marked by IT-4F) to 6.87 nm, suggesting that the aggregation of IT-4F molecules was enhanced after DIO treatment. By contrast, the PM6 neat film (PM6:DIO) only

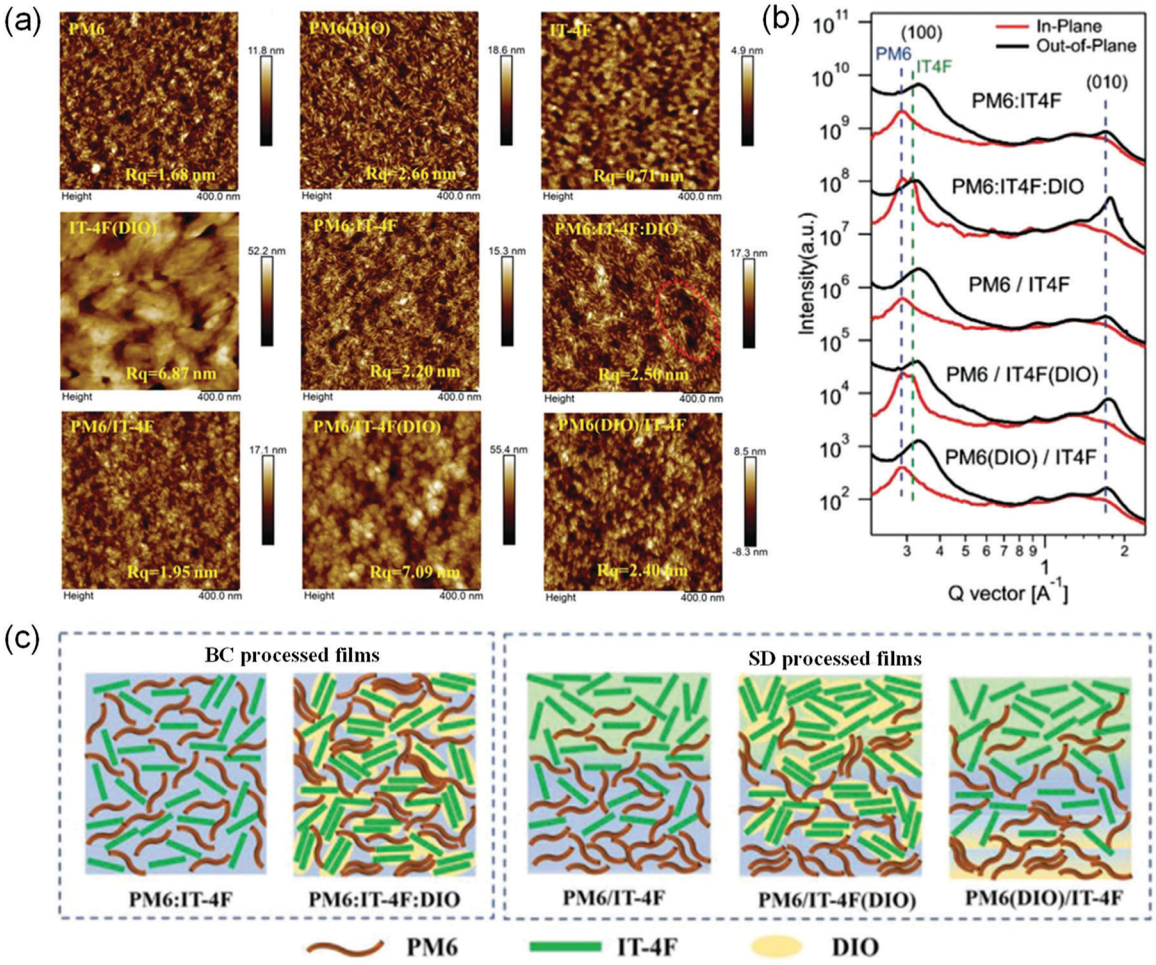

Fig. 5 (a) AFM height images of PM6 neat films, IT-4F neat films, and BC processed PM6:IT-4F blend films and SD processed PM6/IT-4F blend films with and without DIO additive. (b) The out-of-plane and in-plane GIWAXS profiles for the BC and SD processed blend films with and without DIO. (c) Schematic illustration of the morphology of the BC and SD processed blend films with and without DIO. Reproduced with permission.[89] Copyright 2021, Wiley.

Published on 27 April 2021. Downloaded by Yunnan University on 8/23/2025 11:05:38 AM.

displayed a slight increase of R_q from 1.68 nm to 2.66 nm. Similar to the results of the IT-4F neat films, the SD processed blend film with DIO in the IT-4F layer also exhibited a high R_q of 7.04 nm, while the PM6(DIO)/IT-4F film delivered a slightly increased R_q of 2.40 nm, compared to the PM6/IT-4F film (1.95 nm). The AFM results suggest that DIO had a greater impact on the aggregation of IT-4F than PM6. From the GIWAXS results, the crystallinity of PM6 and IT-4F in both PM6/IT-4F(DIO) based SD film and PM6:IT-4F:DIO based BC film was much higher than those in the blend films without DIO, and the crystallinity of IT-4F was improved to a higher degree relative to that of PM6. This result indicates that DIO has a greater influence on the crystallization of IT-4F than polymer PM6, which is consistent with the AFM results. The PM6(DIO)/IT-4F based SD film only showed slightly enhanced crystallinity relative to the SD blend film without DIO, thus affording a similar device performance. Besides, the PM6/IT-4F(DIO) based SD film presented more balanced crystallization of the donor and the acceptor with crystalline balanced factor (the ratio of crystal coherence length (CCL) of the donor and acceptor (100) diffraction of 0.89), which was closer to 1 in comparison to the PM6:IT-4F:DIO based BC film with a lower crystalline balanced factor of 0.61 due to the high crystallinity of IT-4F in the blend. The balanced crystallization of the PM6/IT-4F(DIO) based blend is beneficial for charge transport.

According to the AFM and GIWAXS results, the microstructure of these five films (PM6/IT-4F, PM6/IT-4F(DIO), PM6(DIO)/IT-4F, PM6:IT-4F and PM6:IT-4F:DIO) can be schematically illustrated in Fig. 5c. The greater influence of DIO on the microstructure of IT-4F than that of PM6 could be derived from the higher solubility of IT-4F in DIO. Addition of DIO with high boiling point as the additive provides sufficient time for crystallization of IT-4F, due to the prolonged drying process of the film. Because microcrystalline PM6 can act as the nucleating agent of IT-4F, the crystallinity of IT-4F in the BC processed PM6:IT-4F:DIO film was much higher than that in the SD processed PM6/IT-4F(DIO) film. For the SD processed PM6(DIO)/IT-4F film, the residual DIO in the PM6 layer induced a slight enhancement in the crystallinity of IT-4F at the donor/acceptor interface. Moreover, all the SD processed blend films delivered strong vertical separation with IT-4F enriched on the top and PM6 gathered at the bottom, while the vertical distribution in the BC processed films was relatively uniform. The ideal morphology of the SD processed PM6/IT-4F(DIO) film delivered more balanced crystallization and suitable vertical separation, thus benefiting charge transfer and collection. These results indicate that adding DIO into IT-4F solution is able to improve the crystallinity of the acceptor of the SD processed blend film, and the superior device performance of the PM6/IT-4F(DIO) blend is benefited from the balanced crystallization and suitable vertical separation.

Jen *et al.* employed high-boiling-point CN as the solvent additive to control the morphology of SD processed PM6/Y6-BO film.[90] Similar to the effect of DIO in the PM6/IT-4F blend system discussed above, the incorporation of CN can also extend the film-drying time and promote the crystallization of the small molecule acceptor Y6-BO. Upon addition of CN, the Y6-BO neat film presented significantly improved molecular ordering as confirmed by the appearance of multiple sharp diffraction peaks in the GIWAXS pattern. For the PM6/Y6-BO based SD blend in which the Y6-BO layer was processed with CN as an additive, the crystallinity of Y6-BO was enhanced and the phase separation became more obvious, contributing to efficient charge transport. As a result, the SD device processed with CN exhibited a maximum PCE of 17.2%, which outperformed the device without CN (16.2%). By contrast, the BC processed blend film with CN showed excessive phase separation, and hence achieved an inferior device efficiency of 16.4%. This study suggests that the SD method combined with solvent additive allows the precise control of the crystallinity of non-fullerene acceptor and the phase separation of the blend film.

The high-boiling-point solvent additives can not only regulate the molecular packing and phase separation, but also control the distribution of the donor and acceptor components in the vertical direction. Huang and co-workers deposited the Y6 acceptor layer from the chloroform solution with various contents of DIO as an additive onto the PM6 donor layer.[91] Different from the films with 1% and 2% DIO with rough surface, the blend film without DIO and with 0.5% DIO exhibited smooth surface, as confirmed by the clear Kessing fringes in their neutron reflectivity (NR) profiles (Fig. 6a). This means that a higher content of DIO induced the aggregation of PM6 and Y6, and led to the formation of a coarsened interface in the bulk and on the surface. Besides, with the increase of DIO ratios from 0 to 2%, the SD blend films exhibited a thicker donor/acceptor interdiffusion region, while the change in the transition region from the pure Y6 layer to the interdiffusion layer became more gradual and the donor-enriched and acceptor-enriched layers become thinner (Fig. 6b). The improved donor/acceptor interdiffusion with increased donor/acceptor interface upon addition of DIO was favorable for exciton dissociation. The CCL values of (010) diffraction in the out-of-plane direction for the SD blend films processed with 0, 0.5% and 1% DIO were 19.22, 25.21 and 23.25 Å, respectively. Obviously, the incorporation of DIO induced ordered molecular packing, and the SD film with 0.5% DIO delivered the best crystallinity, which was beneficial for charge transport. The broadened donor/acceptor mixing region and enhanced molecular ordering can be explained by the extended drying process of the acceptor layer with the high-boiling-point additive, which provided more time for the molecular packing and allowed more Y6 molecules to diffuse into the underlying PM6 layer. However, when the relatively high fraction of DIO was added, the crystallization of Y6 molecules could be disturbed by the underlying PM6 due to the serious diffusion between PM6 and Y6, so the crystallinity of the SD blend film with 1% DIO was slightly lower than that of the film with 0.5% DIO. Owing to the coarse donor/acceptor interdiffusion region and ordered molecular packing, the SD blend film with 0.5% DIO showed a high PCE of 16.2%, outperforming the SD blends without DIO or with higher ratios of DIO, as well as the BC processed blend.

 This journal is © The Royal Society of Chemistry and the Chinese Chemical Society 2021

Published on 27 April 2021. Downloaded by Yunnan University on 8/23/2025 11:05:38 AM.

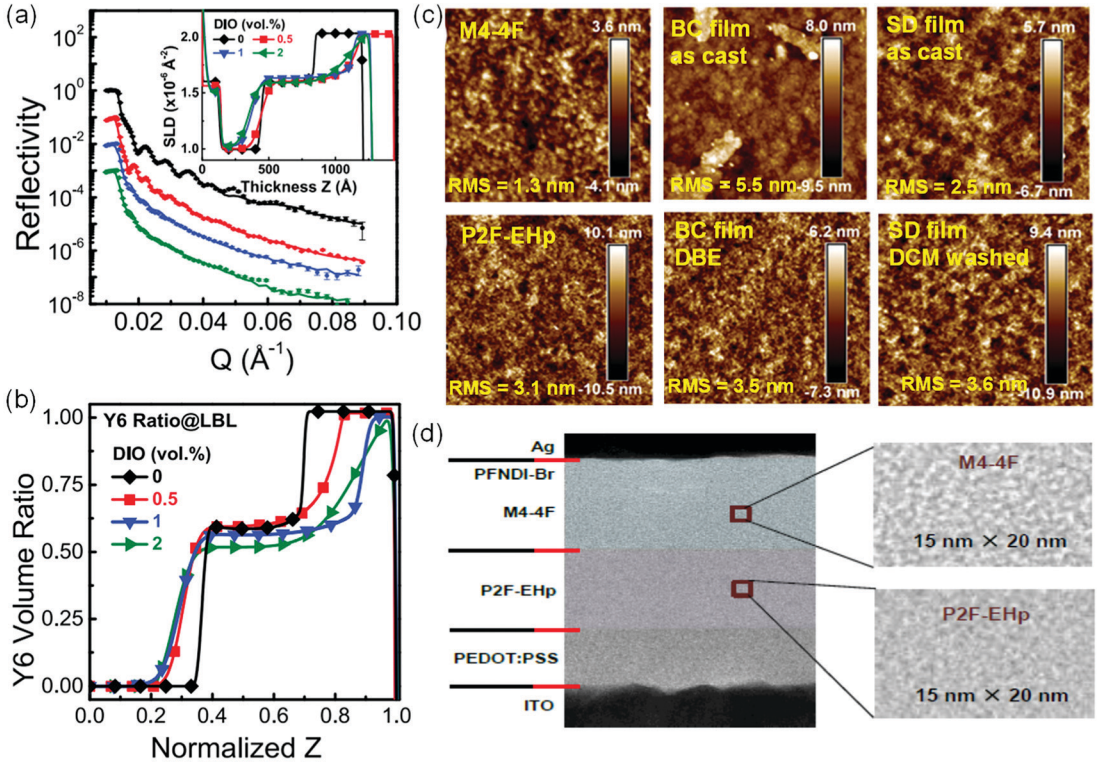

Fig. 6 (a) Neutron reflectivity profiles of SD processed PM6/Y6 films without and with DIO, and corresponding neutron scattering length density (SLD) as a function of film thickness. (b) Volume ratio of Y6 against normalized thickness. Reproduced with permission.[91] Copyright 2020, American Chemical Society. (c) AFM height images (5 × 5 μm) of M4-4F and P2F-EHp neat films, the optimal BC blend film, the optimal SD blend film and the optimal SD blend film washed by DCM. (d) Cross-sectional TEM image of the optimal SD OSC device with enlarged views of P2F-EHp and M4-4F layers. Reproduced with permission.[92] Copyright 2021, Elsevier.

High-boiling-point solvent additives can also be incorporated into the underlying polymer solution to tune the film surface energy and donor/acceptor interdiffusion. Recently, Ying and co-workers prepared an underlying polymer P2F-EHp layer with chloroform as the main solvent and dibenzyl ether (DBE) as the solvent additive, followed by depositing an acceptor M4-4F layer with dichloromethane (DCM).[92] Upon addition of 2% DBE, the PCE of the SD processed OSC devices was significantly increased from 11.85% to 14.21%. The BC processed devices without DBE and with 0.1% DBE showed lower PCEs of 11.72% and 12.77%, respectively. The inferior performance of the BC processed devices can be explained by the excessive phase separation (Fig. 6c), which was related to the low miscibility between P2F-EHp and M4-4F as confirmed by the greatly different surface energy of P2F-EHp (54.41 mN m^{-1}) and M4-4F (16.58 mN m^{-1}) neat films. The poor donor/acceptor miscibility was also detrimental for the permeation of M4-4F into the P2F-EHp layer and the formation of a uniform morphology. Fortunately, when 2% DBE was added into the P2F-EHp solution, the surface energy of the P2F-EHp film was reduced to 27.16 mN m^{-1} and closer to that of M4-4F, increasing the miscibility between the donor and the acceptor. As shown in the AFM images (Fig. 6c), the SD film with 2% DBE showed a uniform surface with a similar roughness to the M4-4 neat film; after washing off the top M4-4 layer of the SD film with DCM, the resulting bottom film presented slightly higher roughness relative to the P2F-EHp neat film. In addition, there was a well-defined boundary between the donor layer and the acceptor layer in the TEM image of the SD processed film with DBE (Fig. 6d). These results indicate that the acceptor molecules permeated to the underlying polymer film and both the donor and acceptor layers maintained high purity in the SD film with DBE. Although the incorporation of DBE improved the performance of both BC and SD processed OSCs, the roles of this additive in morphology manipulation were different. For BC processed blend films, a small amount (*i.e.* 0.1%) of DBE enhanced molecular ordering and domain purity, but a prolonged film drying process also caused excessive aggregation of M4-4F. For the SD processed film, addition of 2% DBE into P2F-EHp solution altered the surface energy of the polymer film and helped the acceptor solution to swell the polymer film, leading to the proper morphology with donor/acceptor intermixing region and pure donor and acceptor phases. Consequently, the SD processed OSCs with 2% DBE afforded the champion efficiency.

As can be seen from the above studies, the solvent additives can be incorporated into any one of the donor and acceptor layers, enabling morphology control in a precise manner. With the high boiling point and good solubility for small molecule acceptors, the solvent additives like DIO and CN can be incorporated into the acceptor solution to improve the molecular crystallinity and donor/acceptor interdiffusion. On the

Published on 27 April 2021. Downloaded by Yunnan University on 8/23/2025 11:05:38 AM.

other hand, the addition of solvent additives like DBE to the solution of underlying polymers is able to change the surface energy of the polymer film and tune its miscibility with acceptors, leading to more suitable film morphology.

2.3 Construction of the ternary active layer

As concluded from the above studies, the SD method can easily prepare favorable distribution of donor and acceptor components in the vertical direction of the film, leading to efficient charge transport and collection with negligible charge recombination loss. Applying the SD method to fabricate ternary OSCs can offer an additional means to increase photovoltaic performance. The ternary SD OSCs can be constructed by incorporating another donor or acceptor component into the donor or acceptor layer of SD film, or sequentially depositing two binary blend layers.

Ma *et al.* used the ternary strategy to regulate the crystallization of polymer donor and small molecule acceptors through sequentially blade-coating PBDB-T:FOIC blend over PBDB-T:IT-M film.[93] From the GIWAXS data, the crystallization coherence length (CCL) of (100) diffraction of PBDB-T in the SD-bladed ternary films (21.26 nm) was higher than those in both binary films of PBDB-T:IT-M (16.07 nm) and PBDB-T:FOIC (16.65 nm), while the CCL value of (100) diffraction of FOIC was decreased from 16.15 nm for the PBDB-T:FOIC binary film to 14.13 nm for the ternary film. These results suggest that the molecular ordering of PBDB-T was significantly enhanced but the crystallization of FOIC was largely depressed. The crystallinity of each component in the vertical direction was also investigated by GIWAXS measurement with different incidence angles. The diffraction peaks of PBDB-T in two binary blend films decreased gradually from the surface to the bottom. However, for the SD processed ternary film, PBDB-T stacking peaks with similar intensity were observed along the vertical direction, indicating that PBDB-T crystals are evenly distributed. In-situ GIWAXS was carried out to understand the morphology development and evolution of crystallization. As shown in Fig. 7a, the film-formation process can be divided into three periods, including dissolved stage (I), nucleation and growth stage (II) and dried film stage (III). All of the binary and ternary

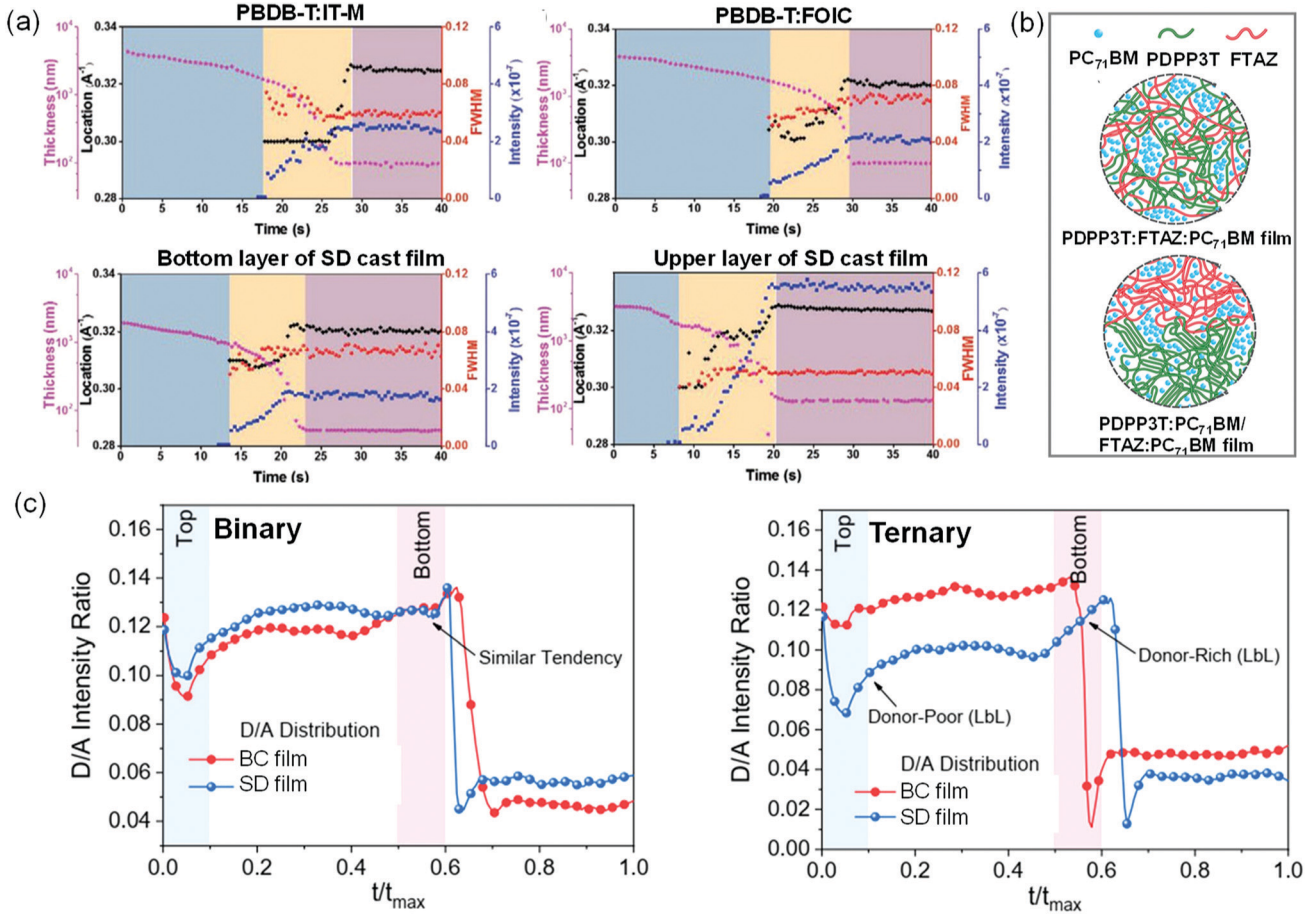

Fig. 7 (a) Evolution of the thickness and the location, the peak full width at half maximum and intensity of the (100) diffraction peaks for BC processed PBDB-T:IT-M and PBDB-T:FOIC films, and bottom and upper layers of SD processed PBDB-T:IT-M/PBDB-T:FOIC film. Reproduced with permission.[93] Copyright 2020, Wiley. (b) Schematic illustration of the morphology of BC processed PDPP3T:FTAZ:$PC_{71}BM$ film and SD processed PDPP3T:$PC_{71}BM$/FTAZ:$PC_{71}BM$ film. Reproduced with permission.[63] Copyright 2016, Wiley. (c) Donor/acceptor intensity ratio (determined by TOF-SIMS ion yields of F^- and CN^-) as a function of sputtering time for PM6:BO-4Cl (or PM6/BO-4Cl) binary films and PM6:BO-4Cl:BTP-S2 (or PM6/BO-4Cl:BTP-S2) ternary films processed with BC and SD methods. Reproduced with permission.[75] Copyright 2021, Wiley.

 This journal is © The Royal Society of Chemistry and the Chinese Chemical Society 2021

Published on 27 April 2021. Downloaded by Yunnan University on 8/23/2025 11:05:38 AM.

blends exhibited similar crystallization behavior during stage I, but different beginning time of stage II, which was 14 s for the bottom PBDB-T:IT-M layer of the SD film, 8 s for the top PBDB-T:FOIC layer of the SD film, and ~18 s for the binary films of PBDB-T:IT-M and PBDB-T:FOIC. Clearly, PBDB-T in the top PBDB-T:FOIC layer of the SD film crystallized much faster than the other films, derived from a large number of polymer crystal nuclei provided by the bottom layer. The accelerated and improved crystallization of PBDB-T contributed to the formation of evenly vertical phase separation. Meanwhile, the improved crystallization of PBDB-T could compete with the crystallization of FOIC, and thus suppress the formation of large FOIC crystals and aggregates. As a result, relatively small domains were observed in the ternary blend film. By contrast, the binary PBDB-T:FOIC film exhibited extensive phase separation due to the strong aggregation characteristics of FOIC. The more proper phase separation and the favorable vertical composition distribution enabled the superior photovoltaic performance (PCE = 11.91%) of the SD processed ternary OSCs, while the two binary devices based on PBDB-T:IT-M and PBDB-T:FOIC showed PCEs of about 10%. This work emphasized the importance of the balanced crystallization kinetics between the polymer donor and small molecule acceptor on the ideal film morphology, which can be realized by the combination of the SD method and ternary strategy.

The miscibility of photoactive materials also plays an important role in morphology control. Understanding the influence of molecular miscibility on morphology has become more and more important for achieving high-performance OSCs. As for ternary blends, the miscibility between components has more complex effects on the film morphology. In 2017, Ade and co-workers studied the miscibility between the three components (PDPP3T, FTAZ and $PC_{71}BM$) in-depth, and fabricated high-performance ternary OSCs.[63] Flory–Higgins interaction parameter (χ), which was estimated using the melting-point depression method, was used as a fundamental metric of molecular miscibility. The χ between PDPP3T and FTAZ was calculated to be a negative value (-0.56), indicating that the two polymers were highly miscible and there was no driving force for the phase separation between them. Thus, the two donor polymers formed mechanical alloys in the PDPP3T:FTAZ:$PC_{71}BM$ based BC ternary film, as schematically illustrated in Fig. 7b. Despite the complementary absorption shown by PDPP3T and FTAZ, the ternary OSC device made by the BC method delivered poor PCEs of 4–5%, which were even lower than those of the BC processed PDPP3T:$PC_{71}BM$ (6.23%) and FTAZ:$PC_{71}BM$ (5.78%) binary devices. Through separately casting the PDPP3T:$PC_{71}BM$ layer (bottom) and FTAZ:$PC_{71}BM$ layer (top), the limitation from material miscibility was overcome and the PCE of the SD processed ternary OSC increased to 6.73%. The phase separation of the PDPP3T:$PC_{71}BM$ layer was hardly affected by the deposition of the FTAZ:$PC_{71}BM$ layer, and the preferred vertical morphology with stacked double BHJ layers was obtained as revealed by Dynamic secondary-ion mass spectroscopy (DSIMS) analysis. This study suggests that the SD method can help to overcome the material-induced limitations and form the desired film morphology that is hardly achieved by processing with a mixed ternary solution.

To tune material miscibility and promote the vertical distribution of the donor and acceptor components in the blend film, Chen *et al.* introduced an asymmetric acceptor BTP-S2 with lower miscibility with polymer PM6 to the binary blend of PM6/BO-4Cl.[75] The SD processed ternary device with a BO-4Cl:BTP-S2 blend layer over the PM6 layer exhibited a high PCE up to 18.16%, which was not only higher than those of the SD and BC processed binary devices but also higher than that of the BC processed ternary device. The difference of the photovoltaic performance can be explained by the film morphology, especially the vertical phase separation in active layers, as confirmed by the time of flight secondary ion mass spectrometry (TOF-SIMS) results. The relative content of the polymer donor and the small molecule acceptors in the vertical direction can be reflected by the intensity ratio of F^-/CN^- variations. As shown in Fig. 7c, both SD and BC processed binary blend films showed the BHJ-like morphology with similar vertical composition distribution. For the SD processed ternary blend film, the strong vertical distribution with PM6 mostly enriched at the bottom and acceptor molecules gathered on the surface were observed. However, the BC processed ternary film presented an even distribution of PM6 and the acceptors. The various vertical distributions of the donor and acceptor components could be derived from the miscibility between the three materials. The χ parameter of PM6 and BTP-S2 estimated by a contact angle method was 0.55, which was higher than those of PM6 and BO-4Cl (0.26), indicative of the lower miscibility between PM6 and BTP-S2. Hence, the incorporation of BTP-S2 into the blend reduces the miscibility between PM6 and the acceptors, as determined by the increased χ value from 0.26 to 0.44. In the process of film preparation using the SD method, the processing solvent (chloroform) for the acceptor will permeate into the PM6 layer, and PM6 might go up and be mixed with the acceptor molecules. Owing to the high miscibility between PM6 and BO-4Cl, a vertically uniform morphology was formed for the SD processed binary film like that processed by the BC method. After incorporating a third component of BTP-S2 with low miscibility with PM6 into the acceptor solution, the floating up of the underlying PM6 could be hindered, resulting in a more suitable phase separation in the vertical direction. The formation of the vertical phase separation in the SD processed ternary blend film improved charge collection and reduced charge recombination, thus affording a superior device performance. This study indicates that tuning the miscibility between donor and acceptor materials by a ternary strategy can regulate the vertical composition distribution in the SD processed blend films and promote the device performance.

Chen's group utilized fullerene acceptor ICBA as the third component to regulate the vertical phase separation of the SD processed PM6/IT-4F blend. Acceptor IT-4F was more miscible with ICBA than that with PM6.[94] Hence, upon addition of ICBA, part of PM6 that was miscible with IT-4F, tended to separate from IT-4F and accumulate at the bottom, and meanwhile the IT-4F was enriched on the film surface, yielding a more obvious

Published on 27 April 2021. Downloaded by Yunnan University on 8/23/2025 11:05:38 AM.

phase separation in the vertical direction. Furthermore, the molecular ordering of PM6 was enhanced as PM6 was partially separated from IT-4F. Consequently, the SD processed ternary PM6/IT-4F:ICBA device possessed efficient charge generation, transport and extraction, offering a PCE of 14.25% that was higher than those of the BC processed binary and ternary devices and the SD processed binary device. To manipulate the morphology and extend the absorption range of the blend of PM6/IT-4F, this group introduced a low-bandgap nonfullerene acceptor F8IC as the third component into the acceptor layer.[95] F8IC has complementary light absorption with the host blend of PM6/IT-4F and good miscibility with IT-4F. Due to the high miscibility, IT-4F and F8IC can form an alloy phase, which facilitated the charge transfer at the donor/acceptor interface. Attributed to the formation of acceptor alloy and the favorable vertical phase separation for the SD processed PM6/IT-4F:F8IC ternary blend, a higher PCE of 14.2% was achieved in comparison to those of the BC processed binary device (13.0%) and ternary device (13.8%). Recently, Alex and co-workers found improved crystallinity of the ternary SD film with the N3:$PC_{71}BM$ blend as the upper layer and PM6 as the lower layer was not only beneficial for charge transport, but also led to increased exciton diffusion length.[96] As a result, the SD processed ternary device showed a higher PCE of 17.42% in comparison to the BC processed ternary device (16.44%).

Yip and co-workers also employed the ternary strategy to regulate molecular ordering and intermixing between of the donor and acceptor materials.[97] They fabricated the SD ternary devices using the three materials with complementary light absorption by depositing IEICO-4F:FBR blend onto the polymer PffBT4T-2OD layer, and also fabricated ternary devices *via* the BC method and binary devices *via* SD and BC methods for comparison. The PCEs of the ternary devices processed with both SD and BC methods were superior to the corresponding binary devices made by the same method, and the SD processed ternary device obtained the best performance with a PCE of 11.3%. The high device performance of the SD and BC processed ternary devices can be ascribed to the improved film morphology, which was induced by the decreased donor/acceptor miscibility and more ordered molecular packing. The PffBT4T-2OD/IEICO-4F blend exhibited poor miscibility with a relatively high χ value of 0.132, while acceptor FBR can be mixed well with both PffBT4T-2OD and IEICO-4F, as confirmed by the small χ values of 0.032 and 0.033, respectively. The introduction of FBR increased the miscibility between the donor and the acceptors, and created more donor/acceptor interfaces for exciton dissociation, resulting in improved photovoltaic performance of the SD and BC ternary devices. However, for the ternary blend processed by the BC method, more PffBT4T-2OD/FBR interface with less efficient exciton dissociation could be formed especially when the content of FBR was high, so the device efficiency was inferior and more sensitive to the content of FBR in comparison to that of the SD processed ternary blend. By contrast, applying the SD method to prepare ternary blend films displayed better control of the location of the third component.

These studies mentioned above suggest that combination of SD deposition method and ternary strategy is a feasible way to optimize the performance of OSCs. The intrinsic properties of the photovoltaic materials, such as crystallinity and miscibility, are the key factors that influence the morphology and the device performance of the SD processed ternary blends. For both SD and BC methods, the introduction of the third photovoltaic material can not only improve light absorption and charge transfer through cascade energy levels, but also tune molecular ordering and phase separation. Nevertheless, the separated coating processes of the donor layer and acceptor layer in the SD method make the morphology control of the ternary blend films simpler and more effective, highlighting the great potential of the SD based ternary strategy in fabricating high-performance OSCs.

3. Stability of SD processed OSCs

In addition to device efficiency, another critical factor for the practical applications of OSCs is performance stability, which is significantly influenced by the morphology of the active layers. In general, there is a large difference in vertical and lateral film morphology between the SD and BC methods. Hence, the OSC devices made by the two methods always exhibit different stability. In this section, we outline the influence of the SD method on the thermal stability and photostability of the film morphology and device performance, and compare the stability of SD processed devices with that of BC processed devices.

To probe the effects of the SD method on thermal stability of OSC devices, Kim *et al.* thoroughly studied the changes in morphology and photovoltaic parameters of SD processed PCPDTBT/$PC_{71}BM$ film under constant thermal stress in comparison to the BC blend film.[69] As shown in Fig. 8a, under continuous heating at 80 °C for 10 days, the PCE of the SD processed devices degraded from 5.03% to 4.89%, which represents 2.8% loss in efficiency. By contrast, the PCE of the blend casting devices significantly dropped from 4.00% to 1.50%, corresponding to a 62.5% efficiency loss. It was observed that the film morphology was not altered significantly in macroscopic scale for both SD and BC blend films upon thermal annealing at 80 °C for 10 days, and the morphological change in the nanoscale could be the reason for the different device stabilities between the two processing methods. As shown in the in-plane GIWAXS profiles (Fig. 8b), the peak full width at half maximum (FWHM) of the (100) and (200) diffraction peaks arising from lamellar packing of PCDTBT in the SD processed blend film was smaller than that in the blend casting film. This suggests that the crystallinity of the polymer is higher in the SD film, probably because $PC_{71}BM$ inclines to diffuse into the amorphous region of PCDTBT when the $PC_{71}BM$ is sequentially deposited onto the polymer layer that already possesses an ordered microstructure. As the heating time extended to 10 days, the FWHM values of the lamellar packing peaks for the SD processed films were barely altered, indicative of no change in the size of the polymer crystals after the constant thermal stress.

 This journal is © The Royal Society of Chemistry and the Chinese Chemical Society 2021

Published on 27 April 2021. Downloaded by Yunnan University on 8/23/2025 11:05:38 AM.

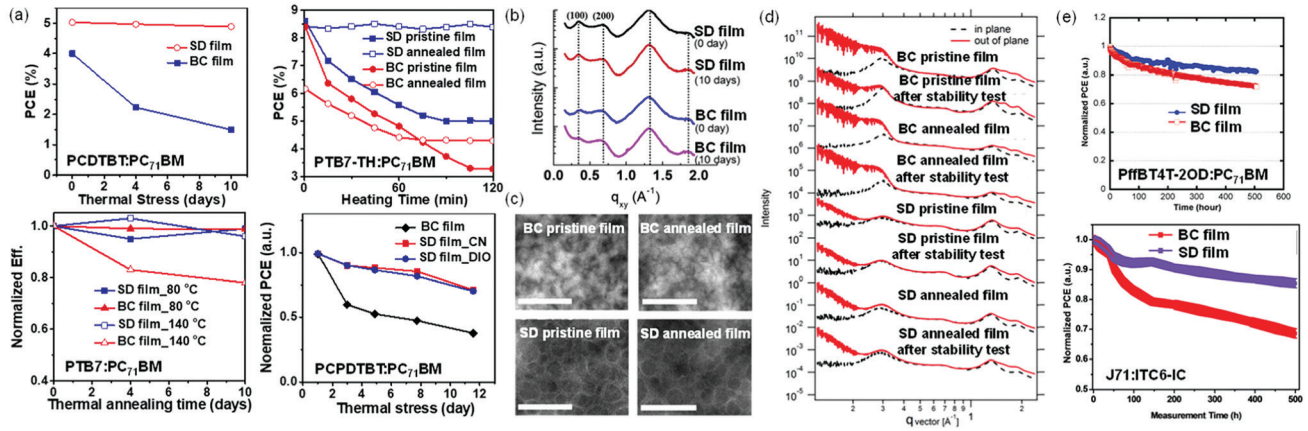

Fig. 8 (a) Variation of PCEs of the SD and BC processed OSCs based on PCDTBT/$PC_{71}BM$, PTB7-TH/$PC_{71}BM$, PTB7/$PC_{71}BM$ and PCPDTBT/$PC_{71}BM$ pairs upon constant thermal stress.[64,67–69] (b) The in-plane GIWAXS profiles for the SD processed PCDTBT/$PC_{71}BM$ film and BC processed PCDTBT:$PC_{71}BM$ film without thermal annealing and with long-term thermal annealing. Reproduced with permission.[69] (c) TEM images of BC processed PTB7-TH/$PC_{71}BM$ film and SD processed PTB7-TH:$PC_{71}BM$ film without treatment and with pre-annealing treatment. The scale bars in all TEM images are 100 nm. (d) The out-of-plane and in-plane GIWAXS profiles for SD processed PTB7-TH/$PC_{71}BM$ film and BC processed PTB7-TH:$PC_{71}BM$ film. Reproduced with permission.[64] Copyright 2016, The Royal Society of Chemistry. (e) Variation of the normalized average PCEs of the SD and BC processed OSCs based on PffBT4T-2OD/$PC_{71}BM$ and J71/ITC6-IC pairs upon continuous illumination (100 mW cm^{-2}). Reproduced with permission.[65,71] Copyright 2019, Wiley. Copyright 2016, The Royal Society of Chemistry.

In contrast, for the blend casting films, the size of ordered domains of the polymer was decreased upon heating for 10 days as revealed by the greatly increased FWHM of the lamellar packing peaks. The result signifies that the $PC_{71}BM$ penetrates the domains of PCDTBT in the blend casting film during the continuous heating process, and renders the polymer phase amorphous. For the SD processed blend film, it becomes more difficult for the $PC_{71}BM$ to diffuse into the PCDTBT domains under constant thermal stress owing to the higher crystallinity of the polymer phase, resulting in improved thermal stability. This study shows the potential of the SD method in achieving thermally stable OSCs.

To improve the thermal stability of SD processed OSCs, Zhan *et al.* carried out pre-annealing treatment (at 100 °C for 20 min before the deposition of electron transport layer and cathode) on the SD processed PTB7-TH/$PC_{71}BM$ blend film, and also fabricated the blend *via* the BC method for comparison.[64] Compared to the BC processed films without and with pre-annealing, superior thermal stability was observed for the SD processed blend films especially for the pre-annealed SD film. After continuous heating at 130 °C for 120 min, the devices based on the BC blends without and with pre-annealing and the SD blend without pre-annealing exhibited ~43%, ~76% and ~60% decrease in PCE, respectively, whereas the efficiency of the device based on the pre-annealed SD blend remained almost unchanged (Fig. 8a). From the TEM images (Fig. 8c), upon the thermal stress, no obvious change in the morphology was observed for the pre-annealed SD film that maintained the dense and continuous polymer networks, which was different from the other three blend films that varied greatly in phase separation scale. As shown in the GIWAXS patterns (Fig. 8d), the pre-annealed SD blend film showed an almost unchanged $PC_{71}BM$ aggregation peak, while the $PC_{71}BM$ aggregation peak was enhanced after the thermal stress for the BC processed blend films and the SD processed blend film without pre-annealing. Fullerene aggregation should be the key reason for the degradation of the OSC devices upon thermal annealing. We infer that the pre-annealing could improve the molecular ordering of PTB7-TH and promote formation of the robust polymer networks which confine the motivation of $PC_{71}BM$. Thus, the fullerene aggregation was suppressed in the pre-annealed SD blend film and the phase-separated film morphology was kept stable under the constant thermal stress.

The SD method also endows the blend systems of PTB7/$PC_{71}BM$[68] and PCPDTBT/$PC_{71}BM$[67] with enhanced thermal stability. To increase the crystallinity of the bottom polymer layer, Kim *et al.* fabricated a polymer PTB7 layer by using a ternary processing solvent comprising CB, DIO and CN, followed by the deposition of a $PC_{71}BM$ layer.[68] For the SD blend film with the ternary solvent, owing to the underlying PTB7 polymer layer with ordered molecular packing, the permeation of $PC_{71}BM$ into the PTB7 layer was suppressed. Thus, the sequential deposition of $PC_{71}BM$ has little impact on the crystallinity of PTB7, and the blend film contained less donor/acceptor intermixed domains, which was beneficial for enhancing morphological stability. By contrast, the blend casting film with higher donor/acceptor intermixing tended to evolve to a thermodynamically stable state with the occurrence of demixing, leading to the poor thermal stability of the morphology.[98–101] After thermal annealing at 140 °C for 10 days, the PCE of the BC device degraded to 78% of its initial value, while the SD device processed with ternary solvent retained 96% of its initial PCE (Fig. 8a). To improve the thermal stability of OSCs with PCPDTBT as a donor and $PC_{71}BM$ as an acceptor, this group fabricated the devices *via* the SD method, and improved the molecular ordering

Published on 27 April 2021. Downloaded by Yunnan University on 8/23/2025 11:05:38 AM.

of the PCPDTBT bottom layer by adding high-boiling-point additive DIO or CN to CB processing solvent.[67] Upon thermal annealing at 80 °C for more than 12 days, both SD devices with DIO and CN as additive exhibited higher stability with ~70% of its initial efficiency, while the BC device only maintained ~40% of its initial efficiency (Fig. 8a).

As concluded from the aforementioned studies, it is easier for the SD processed active layer to obtain the morphology with ordered molecular packing and pure domains, which is beneficial for the formation of the robust polymer network, and thus the achievement of improved thermal stability. However, if the SD method has little impact on the film crystallinity and domain purity, the SD method will fail in enhancing the thermal stability of the devices, such as the PffBT4T-2OD/$PC_{71}BM$ blend with similar thermal stability for the SD and blend casting devices,[65] and PBDB-T/NCBDT blend that even presented inferior thermal stability in the SD device likely due to the unstable interfacial morphology or trap states at the interface.[72] We speculate that the highly ordered polymer phase can be formed *via* the BC method, since the two polymers (PffBT4T-2OD[102] and PBDB-T[103,104]) have temperature-dependent-aggregation behavior in solution.

In practical applications, the solar panels are usually exposed to sunlight for a long period of time, and hence good photostability is necessary for OSCs to be a truly competitive photovoltaic technology. Huang and co-workers investigated the photostability of the OSCs with PffBT4T-2OD as a donor and $PC_{71}BM$ as an acceptor.[65] Although the SD processed devices and the BC devices presented similar thermal stability (as discussed above), improved photostability was observed for the SD processed devices. Under continuous illumination (100 mW cm^{-2}) for 500 h, the PCE of the BC device dropped to 72% of the initial value, while the SD device maintained 83% of its initial PCE (Fig. 8e). The superior photostability of SD processed OSCs is attributed to the vertical film morphology, which allows the fullerene acceptor to hide behind the polymer donor, and reduces the possibility of dimerization of the fullerene under illumination.[66,70] Similarly, the SD processed devices based on the J71/ITC6-IC blend also exhibited higher photostability than their blend casting counterparts, owing to suitable vertical component distribution with more acceptor in the upper part of the active layer.[71] After illumination for 500 h, the PCE of the blend casting device degraded to ~68%, while the PCE of the SD processed device retained ~85% of its initial value (Fig. 8e). These results indicate that the vertical phase separation with the component with lower photostability behind helps the achievement of the photostable SD devices.

As discussed above, the SD method has great potential in constructing thermally stable and photostable OSCs, attributed to the ordered polymer phase and the favorable vertical composition distribution. However, the stability of SD processed OSCs still suffers from a lack of in-depth studies. To advance the commercial application of OSCs, more efforts should be devoted to systematically studying the effects of SD processing on the stability of the OSC devices under various conditions (like heating, illumination and air) and the degradation mechanism.

4. Potential of the SD method in large-area OSCs

With great advantages in finely tuning film microstructure, especially the phase separation in the vertical direction, the SD solution processing method has been proven to be able to fabricate high-performance laboratory-scale OSCs. Currently, the OSC field is in transition, moving away from a focus on laboratory studies towards commercial and cost-effective products. In addition to promoting device efficiency and stability, developing up-scaling techniques for transitioning from small-area laboratory-scale devices to large-area industrial-scale modules is also essential for the commercialization of OSCs.

For fabricating large-area OSC devices, the blade coating technique seems more suitable than the spin-coating method, and has gained considerable attention. By combining the SD method and blade coating technique, Min and co-workers fabricated efficient large-area OSC modules based on PM6:Y6 binary.[74] Different from the BC-bladed film in which Y6 homogeneously distributed throughout the film in the vertical direction, vertical phase separation existed in the SD-bladed blend with Y6 assembled at the top of the film close to the surface air and PM6 enriched in the bottom of the film. In addition, compared to the BC-bladed film, the SD-bladed blend exhibited stronger molecular aggregation and increased phase separation. Owing to the proper film morphology, the SD-bladed OSCs achieved better performance with a small-area (0.04 cm^2) device efficiency of 16.35%, which was higher than that of the small-area BC-bladed OSC device (15.37%). When the area of the SD-bladed device was increased from 0.04 cm^2 to 1 cm^2, the PCE of the SD-bladed device slightly decreased to 15.23%, while the BC-bladed device showed a lower PCE of 14.01%. To probe the compatibility of the SD-bladed method with large-area printing techniques, they also fabricated PM6:Y6 based large-area solar modules with a large area of 11.52 cm^2 (comprising four 35 × 36 mm modules connected in series) in air. Compared to the BC-bladed modules with a PCE of 10.15% and an FF of 50.12%, the SD-bladed modules showed superior performance with a PCE of 11.86% and a FF of 57.85%, which is the record efficiency for large-area OSC modules reported so far. These results indicated that the SD-bladed OSCs presented low sensitivity to the device area, which was partially caused by the suitable film morphology as well as the high photo-absorption rate. Besides, the much higher FF of the large-area SD devices could be related to the decreased series resistance, as shown in Fig. 9b. The lower series resistance for the large-area SD devices could result from the more suitable film morphology, which offered the SD-bladed blend film with more efficient charge transport and extraction with weaker charge recombination. In contrast, for the BC-bladed blend, the donor and acceptor ''islands'' were ineluctable inside the film, and the donor's seeds existed on the cathode side of the film and

 This journal is © The Royal Society of Chemistry and the Chinese Chemical Society 2021

Published on 27 April 2021. Downloaded by Yunnan University on 8/23/2025 11:05:38 AM.

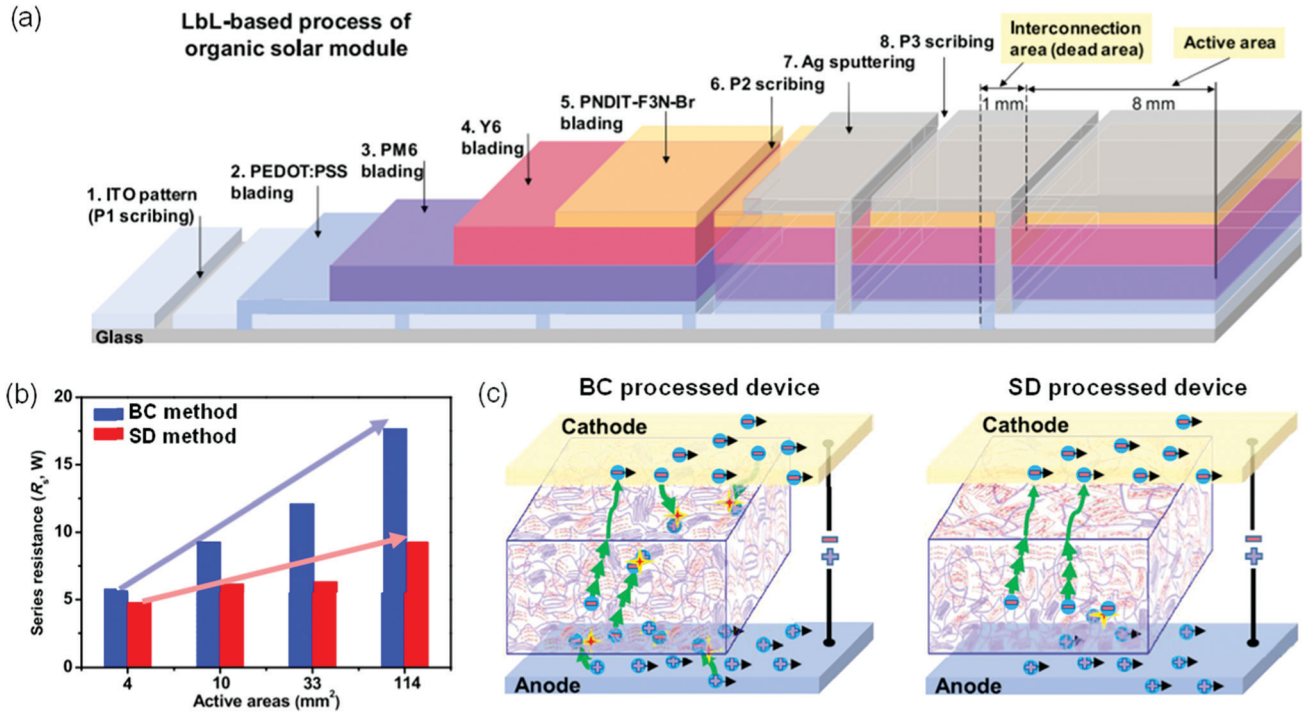

Fig. 9 (a) Process flow diagram of the SD processing for large-area OSC modules. (b) Series resistance values *versus* the device areas for the BC and SD processed OSCs with PM6 as a donor and Y6 as an acceptor. (c) Schematic illustration of the morphology and possible physical dynamics of the BC and SD processed OSCs based on the PM6/Y6 system. Reproduced with permission.[74] Copyright 2020, Elsevier.

the acceptor's seeds existed on the anode side of the film, leading to more serious charge recombination in the bulk and at the interfaces between the active layer and electrodes, as schematically illustrated in Fig. 9c.[74] This study suggests the SD-bladed technique has great potential applied in the high-performance large-area solar modules.

Min *et al.* also adopted the SD-bladed technique to fabricate OSCs based on J71/ITC6-IC and PTQ10/IDIC systems with a device area of 0.04, 0.20, and 1.00 cm^2.[73] Both J71/ITC6-IC and PTQ10/IDIC based devices with an active area of 1.00 cm^2 exhibited PCEs over 10%, showing a slight decrease in comparison with their corresponding small-area (0.04 cm^2) devices (~11%). Huang and co-workers demonstrated the potential of the SD-bladed technique in constructing large-area OSCs, using PffBT4T-2OD/$PC_{71}BM$ and PM6/IT-4F blend systems.[65] When the device area changed from 0.04 cm^2 to 1.00 cm^2, the PCE value decreased from 8.5% to 8.0% for the PffBT4T-2OD/$PC_{71}BM$ SD-bladed device, and from 12.3% to 11.4% for the PM6/IT-4F SD-bladed device. For the BC-bladed devices, both PffBT4T-2OD:$PC_{71}BM$ and PM6:IT-4F blends showed inferior photovoltaic performance with PCEs of 3.8% and 11.2% for the 0.04 cm^2 and 3.0% and 10.6% for the 1.00 cm^2 devices. The film processed using the SD-bladed method showed the desired morphology with favorable vertical composition distribution, resulting in the weakened "islands" of donor and acceptor aggregations and thus less non-geminated recombination, compared to the BC counterparts. As can be seen from these encouraging results, the SD-bladed method is a promising candidate in transitioning up laboratory-scale devices to industrial-scale printed solar modules with minor scaling efficiency gap and good universality (Table 4).

5. Summary and outlook

In this critical review, we overview the recent achievements of SD processed OSCs by analyzing the optimization strategies of film morphology and device performance, and discussing the effects of the SD method on device stability and the performance of large-area devices. The optimization of SD processed OSCs focuses on solvent and solvent additive engineering, and the construction of ternary active layers. The stability and the performance of large-area devices for SD processed OSCs are outlined and compared with the BC processed counterparts.

To simultaneously obtain sufficient donor/acceptor interface and good transport path for electrons and holes for efficient exciton dissociation and charge extraction, the SD method must construct ideal p–i–n like film morphology with suitable lateral and vertical phase separation and high molecular ordering. The ideal film morphology can be achieved by screening suitable processing solvents and introducing solvent additives and the third components. Compared to BC ternary OSCs with complex morphology that is affected by multiple material interactions, the SD method renders morphology control simpler and more precise, enabling increased device performance. Moreover, attributed to the suitable film morphology with pure domains and high crystallinity, the SD method has great potential to make OSC devices with higher thermal and optical

Published on 27 April 2021. Downloaded by Yunnan University on 8/23/2025 11:05:38 AM.

Table 4 The photovoltaic parameters of small-area and large-area OSC devices

Active layer	Processing method	Area (cm^2)	V_{oc} (V)	J_{sc} (mA cm^{-2})	FF (%)	PCE (%)	Ref.
PM6/Y6	SD	0.04	0.834	25.90	75.68	16.35	74
PM6/Y6	SD	1.00	0.831	25.64	71.42	15.23	74
PM6/Y6	SD	11.52	3.20	6.41	57.85	11.86	74
PM6:Y6	BC	0.04	0.840	25.22	72.49	15.37	74
PM6:Y6	BC	1.00	0.835	25.52	65.74	14.01	74
PM6:Y6	BC	11.52	3.21	6.25	50.12	10.15	74
J71/ITC6-IC	SD	0.04	0.960	17.61	67.54	11.42	73
J71/ITC6-IC	SD	0.20	0.971	17.30	66.19	11.13	73
J71/ITC6-IC	SD	1.00	0.973	16.16	65.79	10.35	73
PTQ10/IDIC	SD	0.04	0.952	17.14	69.13	11.28	73
PTQ10/IDIC	SD	0.20	0.963	16.68	69.32	11.13	73
PTQ10/IDIC	SD	1.00	0.965	15.89	67.90	10.42	73
PffBT4T/PC_{71}BM	SD	0.04	0.76	15.80	71	8.2	65
PffBT4T/PC_{71}BM	SD	1.00	0.75	15.4	69	7.8	65
PffBT4T:PC_{71}BM	BC	0.04	0.75	9.50	53	3.4	65
PffBT4T:PC_{71}BM	BC	1.00	0.75	7.6	53	2.8	65
PM6/IT-4F	SD	0.04	0.84	20.7	71	11.9	65
PM6/IT-4F	SD	1.00	0.84	20.0	68	11.0	65
PM6:IT-4F	BC	0.04	0.85	19.7	67	10.8	65
PM6:IT-4F	BC	1.00	0.84	19.5	65	10.1	65

stability, and helps to improve the PCE retention from lab-scale to large-scale devices, making it a significantly promising candidate for OSC commercialization.

Although SD processed OSCs have progressed significantly, the application of the SD processing method remains limited, and record efficiencies are rarely achieved from this processing method, in comparison to the BC method. To further promote the development of SD processed OSCs, there are still some challenging tasks, which are briefly discussed as follows:

(1) Development of solvent selection rules. Compared to the BC method, the SD method is applicable to fewer photovoltaic systems. Due to the similarity in the molecular structure of donor and acceptor materials, it is a rather arduous assignment to select a pair of processing solvents that are suitable for various donors and acceptors. Although considerable efforts have been devoted to solvent engineering, there is still a lack of systematic studies on the general rules for screening processing solvents of both upper and lower layers, which are profoundly desired to make most photovoltaic donor/acceptor blend systems to be prepared *via* the SD method. Hence, it is highly demanded to acquire an in-depth understanding of the effects of the properties (such as solubility, boiling point, ability to swell the polymer, interactions between the solvent and photoactive materials, *etc.*) of the processing solvents on SD film morphology.

(2) Optimization rules for SD processed OSCs. The ideal film morphology especially the favorable vertical phase distribution renders greater potential in achieving high device efficiency *via* the SD method. Currently, the PCEs of the SD processed OSCs have approached or even exceeded those of the BC processed OSCs, but still largely lag behind traditional inorganic solar cells. Various optimization strategies deserve further investigation to increase the performance of SD OSCs. For example, solid additives can be incorporated to control the microstructure of the donor layer or acceptor layer, and a tandem device architecture can be applied to extend the absorption range of SD processed OSCs. Besides, a majority of donor and acceptor materials adopted in SD OSCs are derived from the high-performance BC OSCs; nevertheless, the material matching rules in the two processing methods could be different due to the large difference in the film-forming process. Thus, it is of importance to carry out thorough studies on the donor/acceptor matching rules for SD OSCs.

(3) Comprehensive effects of the SD method on device stability. Although the SD method has shown better potential in multiple donor/acceptor systems, the mechanism of the improved stability still suffers from a lack of comprehensive understanding. Detailed analysis of the morphological features such as lateral and vertical component distribution, crystallinity, and molecular orientation at the donor/acceptor interface, can help us to get more insights into the difference in the stability between SD and BC devices. In addition, the phase diagram can serve as an effective tool to understand the thermodynamic properties of the blends, which significantly affect the morphological stability. Through in-depth studies, the guiding strategies for improving device stability are hoped to be acquired to advance the commercial application of SD OSCs.

(4) Optimizing the performance and stability of low cost OSC systems *via* the SD method. The high cost and poor scalability of synthesis for the current prevailing polymer donors (like PM6, PBDB-T and PTB7-Th) significantly limit the commercialization of OSCs. Therefore, optimization of the polymers with advantages of low cost and ease of syntheses, such as polythiophene and its derivatives,[44,105–119] requires systematic exploration. Limited by the inappropriate donor/acceptor interactions,[106,119,120] the BC processed polythiophene:acceptor blends present unfavorable film morphology and inferior device performance. To overcome the material limitations, the SD method can be introduced to construct the polythiophene/acceptor active layers. By separately manipulating the microstructure of the polythiophene layer and acceptor layers, it can be expected to yield more ideal film morphology. Besides, the stability of the polythiophene-based active layers will also be improved by the SD method, attributed to the formation of enhanced polymer crystallinity and favorable vertical component distribution. Thus, it is possible for the potential low-cost OSC systems to simultaneously achieve high efficiency and good stability, which will enormously advance OSC commercialization.

As a promising alternative to the BC method, the SD method has opened up new opportunities to construct high-performance OSC devices. Through thorough studies on morphology control, device engineering and stability, SD processed OSCs with over 20% efficienciecies will be achieved soon. It is hoped that SD processed OSCs will make a great breakthrough in commercial applications (for instance, solar powered greenhouses, smart buildings).

Author contributions

Miaomiao Li: formal analysis, writing – original draft, funding acquisition. Qi Wang: formal analysis, visualization. Junwei

 This journal is © The Royal Society of Chemistry and the Chinese Chemical Society 2021

Published on 27 April 2021. Downloaded by Yunnan University on 8/23/2025 11:05:38 AM.

Liu: formal analysis, writing – review & editing. Yanhou Geng: writing – review & editing. Long Ye: conceptualization, project administration, supervision, writing – review & editing, funding acquisition.

Conflicts of interest

There are no conflicts to declare.

Acknowledgements

This work was financially supported by the National Natural Science Foundation of China (grant numbers 52073207 and 22075200). L. Y. expresses thanks for the start-up grant of Peiyang Scholar program from Tianjin University and the Open Fund of the State Key Laboratory of Luminescent Materials and Devices (South China University of Technology, No. 2020-skllmd-11).

References

1 C. J. Brabec, Organic photovoltaics: technology and market, *Sol. Energy Mater. Sol. Cells*, 2004, **83**, 273–292.
2 L. Dou, J. You, Z. Hong, Z. Xu, G. Li, R. A. Street and Y. Yang, 25th anniversary article: a decade of organic/polymeric photovoltaic research, *Adv. Mater.*, 2013, **25**, 6642–6671.
3 Z. He, B. Xiao, F. Liu, H. Wu, Y. Yang, S. Xiao, C. Wang, T. P. Russell and Y. Cao, Single-junction polymer solar cells with high efficiency and photovoltage, *Nat. Photonics*, 2015, **9**, 174–179.
4 A. J. Heeger, 25th anniversary article: Bulk heterojunction solar cells: understanding the mechanism of operation, *Adv. Mater.*, 2014, **26**, 10–27.
5 M. Kaltenbrunner, M. S. White, E. D. Glowacki, T. Sekitani, T. Someya, N. S. Sariciftci and S. Bauer, Ultrathin and lightweight organic solar cells with high flexibility, *Nat. Commun.*, 2012, **3**, 770.
6 G. Li, R. Zhu and Y. Yang, Polymer solar cells, *Nat. Photonics*, 2012, **6**, 153–161.
7 L. Lu, T. Zheng, Q. Wu, A. M. Schneider, D. Zhao and L. Yu, Recent Advances in Bulk Heterojunction Polymer Solar Cells, *Chem. Rev.*, 2015, **115**, 12666–12731.
8 M. C. Scharber and N. S. Sariciftci, Efficiency of bulk-heterojunction organic solar cells, *Prog. Polym. Sci.*, 2013, **38**, 1929–1940.
9 R. Søndergaard, M. Hösel, D. Angmo, T. T. Larsen-Olsen and F. C. Krebs, Roll-to-roll fabrication of polymer solar cells, *Mater. Today*, 2012, **15**, 36–49.
10 Y. Zhou, C. Fuentes-Hernandez, T. M. Khan, J. C. Liu, J. Hsu, J. W. Shim, A. Dindar, J. P. Youngblood, R. J. Moon and B. Kippelen, Recyclable organic solar cells on cellulose nanocrystal substrates, *Sci. Rep.*, 2013, **3**, 1536.
11 P. Cheng, G. Li, X. Zhan and Y. Yang, Next-generation organic photovoltaics based on non-fullerene acceptors, *Nat. Photonics*, 2018, **12**, 131–142.
12 J. Hou, O. Inganas, R. H. Friend and F. Gao, Organic solar cells based on non-fullerene acceptors, *Nat. Mater.*, 2018, **17**, 119–128.
13 C. Yan, S. Barlow, Z. Wang, H. Yan, A. K. Y. Jen, S. R. Marder and X. Zhan, Non-fullerene acceptors for organic solar cells, *Nat. Rev. Mater.*, 2018, **3**, 18003.
14 W. Huang, Z. Jiang, K. Fukuda, X. Jiao, C. R. McNeill, T. Yokota and T. Someya, Efficient and Mechanically Robust Ultraflexible Organic Solar Cells Based on Mixed Acceptors, *Joule*, 2020, **4**, 128–141.
15 G. Yu, J. Gao, J. C. Hummelen, F. Wudl and A. J. J. S. Heeger, Polymer Photovoltaic Cells: Enhanced Efficiencies via a Network of Internal Donor-Acceptor Heterojunctions, *Science*, 1995, **270**, 1789–1791.
16 K. Jiang, Q. Wei, J. Y. L. Lai, Z. Peng, H. K. Kim, J. Yuan, L. Ye, H. Ade, Y. Zou and H. Yan, Alkyl Chain Tuning of Small Molecule Acceptors for Efficient Organic Solar Cells, *Joule*, 2019, **3**, 3020–3033.
17 J. Yuan, Y. Zhang, L. Zhou, G. Zhang, H.-L. Yip, T.-K. Lau, X. Lu, C. Zhu, H. Peng, P. A. Johnson, M. Leclerc, Y. Cao, J. Ulanski, Y. Li and Y. Zou, Single-Junction Organic Solar Cell with over 15% Efficiency Using Fused-Ring Acceptor with Electron-Deficient Core, *Joule*, 2019, **3**, 1140–1151.
18 Y. Cui, H. Yao, J. Zhang, K. Xian, T. Zhang, L. Hong, Y. Wang, Y. Xu, K. Ma, C. An, C. He, Z. Wei, F. Gao and J. Hou, Single-Junction Organic Photovoltaic Cells with Approaching 18% Efficiency, *Adv. Mater.*, 2020, **32**, 1908205.
19 Y. Cui, H. Yao, L. Hong, T. Zhang, Y. Tang, B. Lin, K. Xian, B. Gao, C. An, P. Bi, W. Ma and J. Hou, Organic photovoltaic cell with 17% efficiency and superior processability, *Natl. Sci. Rev.*, 2019, **7**, 1239–1246.
20 Q. Liu, Y. Jiang, K. Jin, J. Qin, J. Xu, W. Li, J. Xiong, J. Liu, Z. Xiao, K. Sun, S. Yang, X. Zhang and L. Ding, 18% efficiency organic solar cells, *Sci. Bull.*, 2020, **65**, 272–275.
21 L. Zhu, M. Zhang, G. Zhou, T. Hao, J. Xu, J. Wang, C. Qiu, N. Prine, J. Ali, W. Feng, X. Gu, Z. Ma, Z. Tang, H. Zhu, L. Ying, Y. Zhang and F. Liu, Efficient Organic Solar Cell with 16.88% Efficiency Enabled by Refined Acceptor Crystallization and Morphology with Improved Charge Transfer and Transport Properties, *Adv. Energy Mater.*, 2020, **10**, 1904234.
22 B. Fan, D. Zhang, M. Li, W. Zhong, Z. Zeng, L. Ying, F. Huang and Y. Cao, Achieving over 16% efficiency for single-junction organic solar cells, *Sci. China: Chem.*, 2019, **62**, 746–752.
23 D. Su, M.-A. Pan, Z. Liu, T.-K. Lau, X. Li, F. Shen, S. Huo, X. Lu, A. Xu, H. Yan and C. Zhan, A Trialkylsilylthienyl Chain-Substituted Small-Molecule Acceptor with Higher LUMO Level and Reduced Band Gap for Over 16% Efficiency Fullerene-Free Ternary Solar Cells, *Chem. Mater.*, 2019, **31**, 8908–8917.
24 H. Sun, T. Liu, J. Yu, T.-K. Lau, G. Zhang, Y. Zhang, M. Su, Y. Tang, R. Ma, B. Liu, J. Liang, K. Feng, X. Lu, X. Guo,

Published on 27 April 2021. Downloaded by Yunnan University on 8/23/2025 11:05:38 AM.

F. Gao and H. Yan, A monothiophene unit incorporating both fluoro and ester substitution enabling high-performance donor polymers for non-fullerene solar cells with 16.4% efficiency, *Energy Environ. Sci.*, 2019, **12**, 3328–3337.

25 Y. Cui, H. Yao, J. Zhang, T. Zhang, Y. Wang, L. Hong, K. Xian, B. Xu, S. Zhang, J. Peng, Z. Wei, F. Gao and J. Hou, Over 16% efficiency organic photovoltaic cells enabled by a chlorinated acceptor with increased open-circuit voltages, *Nat. Commun.*, 2019, **10**, 2515.

26 X. Xu, K. Feng, Z. Bi, W. Ma, G. Zhang and Q. Peng, Single-Junction Polymer Solar Cells with 16.35% Efficiency Enabled by a Platinum(II) Complexation Strategy, *Adv. Mater.*, 2019, **31**, 1901872.

27 L. Liu, Y. Kan, K. Gao, J. Wang, M. Zhao, H. Chen, C. Zhao, T. Jiu, A. K. Jen and Y. Li, Graphdiyne Derivative as Multifunctional Solid Additive in Binary Organic Solar Cells with 17.3% Efficiency and High Reproductivity, *Adv. Mater.*, 2020, **32**, 1907604.

28 D. Wang, R. Qin, G. Zhou, X. Li, R. Xia, Y. Li, L. Zhan, H. Zhu, X. Lu, H. L. Yip, H. Chen and C. Z. Li, High-Performance Semitransparent Organic Solar Cells with Excellent Infrared Reflection and See-Through Functions, *Adv. Mater.*, 2020, **32**, 2001621.

29 Y. Zhang, D. Liu, T. K. Lau, L. Zhan, D. Shen, P. W. K. Fong, C. Yan, S. Zhang, X. Lu, C. S. Lee, J. Hou, H. Chen and G. Li, A Novel Wide-Bandgap Polymer with Deep Ionization Potential Enables Exceeding 16% Efficiency in Ternary Nonfullerene Polymer Solar Cells, *Adv. Funct. Mater.*, 2020, **30**, 1910466.

30 S. Li, L. Zhan, Y. Jin, G. Zhou, T. K. Lau, R. Qin, M. Shi, C. Z. Li, H. Zhu, X. Lu, F. Zhang and H. Chen, Asymmetric Electron Acceptors for High-Efficiency and Low-Energy-Loss Organic Photovoltaics, *Adv. Mater.*, 2020, **32**, 2001160.

31 X. Guo, Q. Fan, J. Wu, G. Li, Z. Peng, W. Su, J. Lin, L. Hou, Y. Qin, H. Ade, L. Ye, M. Zhang and Y. Li, Optimized Active Layer Morphologies via Ternary Copolymerization of Polymer Donors for 17.6% Efficiency Organic Solar Cells with Enhanced Fill Factor, *Angew. Chem., Int. Ed.*, 2021, **60**, 2322–2329.

32 Y. Lin, Y. Firdaus, F. H. Isikgor, M. I. Nugraha, E. Yengel, G. T. Harrison, R. Hallani, A. El-Labban, H. Faber, C. Ma, X. Zheng, A. Subbiah, C. T. Howells, O. M. Bakr, I. McCulloch, S. D. Wolf, L. Tsetseris and T. D. Anthopoulos, Self-Assembled Monolayer Enables Hole Transport Layer-Free Organic Solar Cells with 18% Efficiency and Improved Operational Stability, *ACS Energy Lett.*, 2020, **5**, 2935–2944.

33 J. Song, C. Li, L. Zhu, J. Guo, J. Xu, X. Zhang, K. Weng, K. Zhang, J. Min, X. Hao, Y. Zhang, F. Liu and Y. Sun, Ternary Organic Solar Cells with Efficiency >16.5% Based on Two Compatible Nonfullerene Acceptors, *Adv. Mater.*, 2019, **31**, 1905645.

34 Q. An, X. Ma, J. Gao and F. Zhang, Solvent additive-free ternary polymer solar cells with 16.27% efficiency, *Sci. Bull.*, 2019, **64**, 504–506.

35 L. Meng, Y. Zhang, X. Wan, C. Li, X. Zhang, Y. Wang, X. Ke, Z. Xiao, L. Ding, R. Xia, H. L. Yip, Y. Cao and Y. Chen, Organic and solution-processed tandem solar cells with 17.3% efficiency, *Science*, 2018, **361**, 1094–1098.

36 N. D. Treat and M. L. Chabinyc, Phase Separation in Bulk Heterojunctions of Semiconducting Polymers and Fullerenes for Photovoltaics, *Annu. Rev. Phys. Chem.*, 2014, **65**, 59–81.

37 Y. Huang, E. J. Kramer, A. J. Heeger and G. C. J. C. R. Bazan, Bulk heterojunction solar cells: morphology and performance relationships, *Chem. Rev.*, 2014, **114**, 7006–7043.

38 S. Shoaee, M. Stolterfoht and D. Neher, The Role of Mobility on Charge Generation, Recombination, and Extraction in Polymer-Based Solar Cells, *Adv. Energy Mater.*, 2018, **8**, 1703355.

39 C. J. Schaffer, C. M. Palumbiny, M. A. Niedermeier, C. Jendrzejewski, G. Santoro, S. V. Roth and P. Muller-Buschbaum, A direct evidence of morphological degradation on a nanometer scale in polymer solar cells, *Adv. Mater.*, 2013, **25**, 6760–6764.

40 C. J. Brabec, M. Heeney, I. McCulloch and J. Nelson, Influence of blend microstructure on bulk heterojunction organic photovoltaic performance, *Chem. Soc. Rev.*, 2011, **40**, 1185–1199.

41 M. Gao, Z. Liang, Y. Geng and L. Ye, Significance of thermodynamic interaction parameters in guiding the optimization of polymer:nonfullerene solar cells, *Chem. Commun.*, 2020, **56**, 12463–12478.

42 X. Li, X. Du, J. Zhao, H. Lin, C. Zheng and S. Tao, Layer-by-Layer Solution Processing Method for Organic Solar Cells, *Sol. RRL*, 2020, **5**, 2000592.

43 Y. Yu, R. Sun, T. Wang, X. Yuan, Y. Wu, Q. Wu, M. Shi, W. Yang, X. Jiao and J. Min, Improving Photovoltaic Performance of Non-Fullerene Polymer Solar Cells Enables by Fine-Tuning Blend Microstructure via Binary Solvent Mixtures, *Adv. Funct. Mater.*, 2020, **31**, 2008767.

44 Q. Wang, Y. Qin, M. Li, L. Ye and Y. Geng, Molecular Engineering and Morphology Control of Polythiophene:-Nonfullerene Acceptor Blends for High-Performance Solar Cells, *Adv. Energy Mater.*, 2020, **10**, 2002572.

45 M. Gao, W. Wang, J. Hou and L. Ye, Control of Aggregated Structure of Photovoltaic Polymers for High-Efficiency Solar Cells, *Aggregate*, 2021, DOI: 10.1002/agt1002.1046.

46 Y. Wang, J. Lee, X. Hou, C. Labanti, J. Yan, E. Mazzolini, A. Parhar, J. Nelson, J. S. Kim and Z. Li, Recent Progress and Challenges toward Highly Stable Nonfullerene Acceptor-Based Organic Solar Cells, *Adv. Energy Mater.*, 2020, **11**, 2003002.

47 F. Zhao, H. Zhang, R. Zhang, J. Yuan, D. He, Y. Zou and F. Gao, Emerging Approaches in Enhancing the Efficiency and Stability in Non-Fullerene Organic Solar Cells, *Adv. Energy Mater.*, 2020, **10**, 2002746.

48 Y. Yao, J. Hou, Z. Xu, G. Li and Y. Yang, Effects of Solvent Mixtures on the Nanoscale Phase Separation in Polymer Solar Cells, *Adv. Funct. Mater.*, 2008, **18**, 1783–1789.

49 T. Song, Z. Wu, Y. Tu, Y. Jin and B. Sun, Vertical phase segregation of hybrid poly(3-hexylthiophene) and fullerene derivative composites controlled via velocity of solvent drying, *Semicond. Sci. Technol.*, 2011, **26**, 034009.

 This journal is © The Royal Society of Chemistry and the Chinese Chemical Society 2021

Published on 27 April 2021. Downloaded by Yunnan University on 8/23/2025 11:05:38 AM.

50 T. H. Lee, S. Y. Park, X. Du, S. Park, K. Zhang, N. Li, S. Cho, C. J. Brabec and J. Y. Kim, Effects on Photovoltaic Characteristics by Organic Bilayer- and Bulk-Heterojunctions: Energy Losses, Carrier Recombination and Generation, *ACS Appl. Mater. Interfaces*, 2020, **12**, 55945–55953.
51 S. Inaba and V. Vohra, Fabrication Processes to Generate Concentration Gradients in Polymer Solar Cell Active Layers, *Materials*, 2017, **10**, 518.
52 B. Gao, Theoretical analysis and the morphology control of vertical phase segregation in high-efficiency polymer/fullerene solar cells, *High Perfom. Polym.*, 2014, **26**, 197–204.
53 V. Vohra, K. Higashimine, S. Tsuzaki, K. Ohdaira and H. Murata, Formation of vertical concentration gradients in poly(3-hexylthiophene-2,5-diyl): Phenyl-C61-butyric acid methyl ester-graded bilayer solar cells, *Thin Solid Films*, 2014, **554**, 41–45.
54 N. Wang, X. Long, Z. Ding, J. Feng, B. Lin, W. Ma, C. Dou, J. Liu and L. Wang, Improving Active Layer Morphology of All-Polymer Solar Cells by Dissolving the Two Polymers Individually, *Macromolecules*, 2019, **52**, 2402–2410.
55 Y. Wang and X. Zhan, Layer-by-Layer Processed Organic Solar Cells, *Adv. Energy Mater.*, 2016, **6**, 1600414.
56 Y. Xu, J. Yuan, S. Liang, J.-D. Chen, Y. Xia, B. W. Larson, Y. Wang, G. M. Su, Y. Zhang, C. Cui, M. Wang, H. Zhao and W. Ma, Simultaneously Improved Efficiency and Stability in All-Polymer Solar Cells by a P–i–N Architecture, *ACS Energy Lett.*, 2019, **4**, 2277–2286.
57 S. A. Hawks, J. C. Aguirre, L. T. Schelhas, R. J. Thompson, R. C. Huber, A. S. Ferreira, G. Zhang, A. A. Herzing, S. H. Tolbert and B. J. Schwartz, Comparing Matched Polymer:-Fullerene Solar Cells Made by Solution-Sequential Processing and Traditional Blend Casting: Nanoscale Structure and Device Performance, *J. Phys. Chem. C*, 2014, **118**, 17413–17425.
58 J. Seok, T. J. Shin, S. Park, C. Cho, J. Y. Lee, D. Yeol Ryu, M. H. Kim and K. Kim, Efficient organic photovoltaics utilizing nanoscale heterojunctions in sequentially deposited polymer/fullerene bilayer, *Sci. Rep.*, 2015, **5**, 8373.
59 X. Zhang, Y. Li, D. Zhang, G. Wu, H. Zhang, J. Zhou, X. Li, Z. Saud uz, J. Zhang, Z. Wei, H. Zhou and Y. Zhang, Molecular dispersion enhances photovoltaic efficiency and thermal stability in quasi-bilayer organic solar cells, *Sci. China: Chem.*, 2020, **64**, 116–126.
60 S. Liang, Z. Lou, Q. Zhang, Y. Xu, F. Jin, J. Yuan, C. Sheng, W. Ma and H. Zhao, Improved Hole Transfer and Charge Generation in All-Polymer Photovoltaic Blends with a P–i–N Structure, *J. Phys. Chem. C*, 2020, **124**, 25262–25269.
61 M. D. M. Faure and B. H. Lessard, Layer-by-layer fabrication of organic photovoltaic devices: material selection and processing conditions, *J. Mater. Chem. C*, 2021, **9**, 14–40.
62 H. Huang, X. Li, C. Sun, I. Angunawela, B. Qiu, J. Du, S. Qin, L. Meng, Z. Zhang, H. Ade and Y. Li, Green solvent-processed organic solar cells based on a low cost polymer donor and a small molecule acceptor, *J. Mater. Chem. C*, 2020, **8**, 7718–7724.
63 M. Ghasemi, L. Ye, Q. Zhang, L. Yan, J. H. Kim, O. Awartani, W. You, A. Gadisa and H. Ade, Panchromatic Sequentially Cast Ternary Polymer Solar Cells, *Adv. Mater.*, 2017, **29**, 1604603.
64 P. Cheng, C. Yan, Y. Wu, S. Dai, W. Ma and X. Zhan, Efficient and stable organic solar cells via a sequential process, *J. Mater. Chem. C*, 2016, **4**, 8086–8093.
65 S. Dong, K. Zhang, B. Xie, J. Xiao, H.-L. Yip, H. Yan, F. Huang and Y. Cao, High-Performance Large-Area Organic Solar Cells Enabled by Sequential Bilayer Processing via Nonhalogenated Solvents, *Adv. Energy Mater.*, 2019, **9**, 1802832.
66 T. Heumueller, W. R. Mateker, A. Distler, U. F. Fritze, R. Cheacharoen, W. H. Nguyen, M. Biele, M. Salvador, M. von Delius, H.-J. Egelhaaf, M. D. McGehee and C. J. Brabec, Morphological and electrical control of fullerene dimerization determines organic photovoltaic stability, *Energy Environ. Sci.*, 2016, **9**, 247–256.
67 H. Hwang, H. Lee, S. Shafian, W. Lee, J. Seok, K. Y. Ryu, D. Yeol Ryu and K. Kim, Thermally Stable Bulk Heterojunction Prepared by Sequential Deposition of Nanostructured Polymer and Fullerene, *Polymers*, 2017, **9**, 456.
68 Y. Jang, Y. Ju Cho, M. Kim, J. Seok, H. Ahn and K. Kim, Formation of Thermally Stable Bulk Heterojunction by Reducing the Polymer and Fullerene Intermixing, *Sci. Rep.*, 2017, **7**, 9690.
69 M. Kim, S. Park, D. Y. Ryu and K. Kim, Improving thermal stability of organic photovoltaics via constructing interdiffused bilayer of polymer/fullerene, *Polymer*, 2016, **103**, 132–139.
70 H. K. H. Lee, A. M. Telford, J. A. Röhr, M. F. Wyatt, B. Rice, J. Wu, A. de Castro Maciel, S. M. Tuladhar, E. Speller, J. McGettrick, J. R. Searle, S. Pont, T. Watson, T. Kirchartz, J. R. Durrant, W. C. Tsoi, J. Nelson and Z. Li, The role of fullerenes in the environmental stability of polymer:fullerene solar cells, *Energy Environ. Sci.*, 2018, **11**, 417–428.
71 R. Sun, J. Guo, Q. Wu, Z. Zhang, W. Yang, J. Guo, M. Shi, Y. Zhang, S. Kahmann, L. Ye, X. Jiao, M. A. Loi, Q. Shen, H. Ade, W. Tang, C. J. Brabec and J. Min, A multi-objective optimization-based layer-by-layer blade-coating approach for organic solar cells: rational control of vertical stratification for high performance, *Energy Environ. Sci.*, 2019, **12**, 3118–3132.
72 J. Zhang, B. Kan, A. J. Pearson, A. J. Parnell, J. F. K. Cooper, X.-K. Liu, P. J. Conaghan, T. R. Hopper, Y. Wu, X. Wan, F. Gao, N. C. Greenham, A. A. Bakulin, Y. Chen and R. H. Friend, Efficient non-fullerene organic solar cells employing sequentially deposited donor–acceptor layers, *J. Mater. Chem. A*, 2018, **6**, 18225–18233.
73 R. Sun, J. Guo, C. Sun, T. Wang, Z. Luo, Z. Zhang, X. Jiao, W. Tang, C. Yang, Y. Li and J. Min, A universal layer-by-layer solution-processing approach for efficient non-fullerene organic solar cells, *Energy Environ. Sci.*, 2019, **12**, 384–395.
74 R. Sun, Q. Wu, J. Guo, T. Wang, Y. Wu, B. Qiu, Z. Luo, W. Yang, Z. Hu, J. Guo, M. Shi, C. Yang, F. Huang, Y. Li and J. Min, A Layer-by-Layer Architecture for Printable Organic Solar Cells Overcoming the Scaling Lag of Module Efficiency, *Joule*, 2020, **4**, 407–419.

Published on 27 April 2021. Downloaded by Yunnan University on 8/23/2025 11:05:38 AM.

75 L. Zhan, S. Li, X. Xia, Y. Li, X. Lu, L. Zuo, M. Shi and H. Chen, Layer-by-Layer Processed Ternary Organic Photovoltaics with Efficiency over 18%, *Adv. Mater.*, 2021, **33**, 2007231.

76 A. N. Bartynski, C. Trinh, A. Panda, K. Bergemann, B. E. Lassiter, J. D. Zimmerman, S. R. Forrest and M. E. Thompson, A fullerene-based organic exciton blocking layer with high electron conductivity, *Nano Lett.*, 2013, **13**, 3315–3320.

77 A. Ojala, A. Petersen, A. Fuchs, R. Lovrincic, C. Pölking, J. Trollmann, J. Hwang, C. Lennartz, H. Reichelt, H. W. Höffken, A. Pucci, P. Erk, T. Kirchartz and F. Würthner, Merocyanine/C60 Planar Heterojunction Solar Cells: Effect of Dye Orientation on Exciton Dissociation and Solar Cell Performance, *Adv. Funct. Mater.*, 2012, **22**, 86–96.

78 K. Cnops, G. Zango, J. Genoe, P. Heremans, M. V. Martinez-Diaz, T. Torres and D. Cheyns, Energy Level Tuning of Non-Fullerene Acceptors in Organic Solar Cells, *J. Am. Chem. Soc.*, 2015, **137**, 8991–8997.

79 S. Yoo, B. Domercq and B. Kippelen, Efficient thin-film organic solar cells based on pentacene/C60 heterojunctions, *Appl. Phys. Lett.*, 2004, **85**, 5427–5429.

80 C. W. Tang, Two-layer organic photovoltaic cell, *Appl. Phys. Lett.*, 1986, **48**, 183–185.

81 J. C. Aguirre, S. A. Hawks, A. S. Ferreira, P. Yee, S. Subramaniyan, S. A. Jenekhe, S. H. Tolbert and B. J. Schwartz, Sequential Processing for Organic Photovoltaics: Design Rules for Morphology Control by Tailored Semi-Orthogonal Solvent Blends, *Adv. Energy Mater.*, 2015, **5**, 1402020.

82 Y. Cui, S. Zhang, N. Liang, J. Kong, C. Yang, H. Yao, L. Ma and J. Hou, Toward Efficient Polymer Solar Cells Processed by a Solution-Processed Layer-By-Layer Approach, *Adv. Mater.*, 2018, e1802499.

83 J. J. van Franeker, S. Kouijzer, X. Lou, M. Turbiez, M. M. Wienk and R. A. J. Janssen, Depositing Fullerenes in Swollen Polymer Layers via Sequential Processing of Organic Solar Cells, *Adv. Energy Mater.*, 2015, **5**, 1500464.

84 W. A. Scrivens and J. M. Tour, Potent Solvents for CG0 and Their Utility for the Rapid Acquisition of 1% NMR Data for Fu llerenes, *J. Chem. Soc., Chem. Commun.*, 1993, **15**, 1207–1209.

85 L. Arunagiri, G. Zhang, H. Hu, H. Yao, K. Zhang, Y. Li, P. C. Y. Chow, H. Ade and H. Yan, Temperature-Dependent Aggregation Donor Polymers Enable Highly Efficient Sequentially Processed Organic Photovoltaics Without the Need of Orthogonal Solvents, *Adv. Funct. Mater.*, 2019, **29**, 1902478.

86 K. Weng, L. Ye, L. Zhu, J. Xu, J. Zhou, X. Feng, G. Lu, S. Tan, F. Liu and Y. Sun, Optimized active layer morphology toward efficient and polymer batch insensitive organic solar cells, *Nat. Commun.*, 2020, **11**, 2855.

87 L. Ye, Y. Xiong, Z. Chen, Q. Zhang, Z. Fei, R. Henry, M. Heeney, B. T. O'Connor, W. You and H. Ade, Sequential Deposition of Organic Films with Eco-Compatible Solvents Improves Performance and Enables Over 12%-Efficiency Nonfullerene Solar Cells, *Adv. Mater.*, 2019, **31**, 1808153.

88 Y. Wei, J. Yu, L. Qin, H. Chen, X. Wu, Z. Wei, X. Zhang, L. Ding, F. Gao and H. Huang, A universal method for constructing high efficiency organic solar cells with stacked structures, *Energy Environ. Sci.*, 2021, **14**, 2314–2321.

89 Q. He, W. Sheng, M. Zhang, G. Xu, P. Zhu, H. Zhang, Z. Yao, F. Gao, F. Liu, X. Liao and Y. Chen, Revealing Morphology Evolution in Highly Efficient Bulk Heterojunction and Pseudo-Planar Heterojunction Solar Cells by Additives Treatment, *Adv. Energy Mater.*, 2021, **11**, 2003390.

90 H. Fu, W. Gao, Y. Li, F. Lin, X. Wu, J. H. Son, J. Luo, H. Y. Woo, Z. Zhu and A. K. Y. Jen, A Generally Applicable Approach Using Sequential Deposition to Enable Highly Efficient Organic Solar Cells, *Small Methods*, 2020, **4**, 2000687.

91 Q. Li, L.-M. Wang, S. Liu, L. Guo, S. Dong, G. Ma, Z. Cao, X. Zhan, X. Gu, T. Zhu, Y.-P. Cai and F. Huang, Vertical Composition Distribution and Crystallinity Regulations Enable High-Performance Polymer Solar Cells with >17% Efficiency, *ACS Energy Lett.*, 2020, **5**, 3637–3646.

92 D. Zhang, W. Zhong, L. Ying, B. Fan, M. Li, Z. Gan, Z. Zeng, D. Chen, N. Li, F. Huang and Y. Cao, Overcoming Incompatibility of Donors and Acceptors by Constructing Planar Heterojunction Organic Solar Cells, *Nano Energy*, 2021, **85**, 105957.

93 Y. Wang, X. Wang, B. Lin, Z. Bi, X. Zhou, H. B. Naveed, K. Zhou, H. Yan, Z. Tang and W. Ma, Achieving Balanced Crystallization Kinetics of Donor and Acceptor by Sequential-Blade Coated Double Bulk Heterojunction Organic Solar Cells, *Adv. Energy Mater.*, 2020, **10**, 2000826.

94 S. Liu, D. Chen, X. Hu, Z. Xing, J. Wan, L. Zhang, L. Tan, W. Zhou and Y. Chen, Printable and Large-Area Organic Solar Cells Enabled by a Ternary Pseudo-Planar Heterojunction Strategy, *Adv. Funct. Mater.*, 2020, **30**, 2003223.

95 J. Wan, L. Zhang, Q. He, S. Liu, B. Huang, L. Hu, W. Zhou and Y. Chen, High-Performance Pseudoplanar Heterojunction Ternary Organic Solar Cells with Nonfullerene Alloyed Acceptor, *Adv. Funct. Mater.*, 2020, **30**, 1909760.

96 K. Jiang, J. Zhang, Z. Peng, F. Lin, S. Wu, Z. Li, Y. Chen, H. Yan, H. Ade, Z. Zhu and A. K. Jen, Pseudo-bilayer architecture enables high-performance organic solar cells with enhanced exciton diffusion length, *Nat. Commun.*, 2021, **12**, 468.

97 M. Ren, G. Zhang, Z. Chen, J. Xiao, X. Jiao, Y. Zou, H. L. Yip and Y. Cao, High-Performance Ternary Organic Solar Cells with Controllable Morphology via Sequential Layer-by-Layer Deposition, *ACS Appl. Mater. Interfaces*, 2020, **12**, 13077–13086.

98 P. Cheng and X. Zhan, Stability of organic solar cells: challenges and strategies, *Chem. Soc. Rev.*, 2016, **45**, 2544–2582.

99 S. A. Gevorgyan, M. V. Madsen, B. Roth, M. Corazza, M. Hösel, R. R. Søndergaard, M. Jørgensen and F. C. Krebs, Lifetime of Organic Photovoltaics: Status and Predictions, *Adv. Energy Mater.*, 2016, **6**, 1501298.

100 N. Li, I. McCulloch and C. J. Brabec, Analyzing the efficiency, stability and cost potential for fullerene-free

 This journal is © The Royal Society of Chemistry and the Chinese Chemical Society 2021

Published on 27 April 2021. Downloaded by Yunnan University on 8/23/2025 11:05:38 AM.

organic photovoltaics in one figure of merit, *Energy Environ. Sci.*, 2018, **11**, 1355–1361.

101 E. M. Speller, A. J. Clarke, J. Luke, H. K. H. Lee, J. R. Durrant, N. Li, T. Wang, H. C. Wong, J.-S. Kim, W. C. Tsoi and Z. Li, From fullerene acceptors to non-fullerene acceptors: prospects and challenges in the stability of organic solar cells, *J. Mater. Chem. A*, 2019, **7**, 23361–23377.

102 Y. Liu, J. Zhao, Z. Li, C. Mu, W. Ma, H. Hu, K. Jiang, H. Lin, H. Ade and H. Yan, Aggregation and morphology control enables multiple cases of high-efficiency polymer solar cells, *Nat. Commun.*, 2014, **5**, 5293.

103 D. Qian, L. Ye, M. Zhang, Y. Liang, L. Li, Y. Huang, X. Guo, S. Zhang, Z. A. Tan and J. Hou, Design, Application, and Morphology Study of a New Photovoltaic Polymer with Strong Aggregation in Solution State, *Macromolecules*, 2012, **45**, 9611–9617.

104 W. Zhao, D. Qian, S. Zhang, S. Li, O. Inganas, F. Gao and J. Hou, Fullerene-Free Polymer Solar Cells with over 11% Efficiency and Excellent Thermal Stability, *Adv. Mater.*, 2016, **28**, 4734–4739.

105 P. Bi, J. Ren, S. Zhang, J. Wang and J. Hou, PTV-based p-type organic semiconductors: Candidates for low-cost photovoltaic donors with simple synthetic routes, *Polymer*, 2020, **209**, 122900.

106 Z. Liang, M. Li, Q. Wang, Y. Qin, S. J. Stuard, Z. Peng, Y. Deng, H. Ade, L. Ye and Y. Geng, Optimization Requirements of Efficient Polythiophene:Nonfullerene Organic Solar Cells, *Joule*, 2020, **4**, 1278–1295.

107 J. Ren, P. Bi, J. Zhang, J. Liu, J. Wang, Y. Xu, Z. Wei, S. Zhang and J. Hou, Molecular design revitalizes the low-cost PTV-polymer for highly efficient organic solar cells, *Natl. Sci. Rev.*, 2021, DOI: 10.1093/nsr/nwab031.

108 Q. Wang, M. Li, Z. Peng, N. Kirby, Y. Deng, L. Ye and Y. Geng, Calculation aided miscibility manipulation enables highly efficient polythiophene:nonfullerene photovoltaic cells, *Sci. China: Chem.*, 2021, **64**, 478–487.

109 Q. Wang, M. Li, X. Zhang, Y. Qin, J. Wang, J. Zhang, J. Hou, R. A. J. Janssen and Y. Geng, Carboxylate-Substituted Polythiophenes for Efficient Fullerene-Free Polymer Solar Cells: The Effect of Chlorination on Their Properties, *Macromolecules*, 2019, **52**, 4464–4474.

110 X. Xu, G. Zhang, L. Yu, R. Li and Q. Peng, P3HT-Based Polymer Solar Cells with 8.25% Efficiency Enabled by a Matched Molecular Acceptor and Smart Green-Solvent Processing Technology, *Adv. Mater.*, 2019, **31**, 1906045.

111 C. Yang, S. Zhang, J. Ren, M. Gao, P. Bi, L. Ye and J. Hou, Molecular design of a non-fullerene acceptor enables a P3HT-based organic solar cell with 9.46% efficiency, *Energy Environ. Sci.*, 2020, **13**, 2864–2869.

112 H. Zhang, S. Li, B. Xu, H. Yao, B. Yang and J. Hou, Fullerene-free polymer solar cell based on a polythiophene derivative with an unprecedented energy loss of less than 0.5 eV, *J. Mater. Chem. A*, 2016, **4**, 18043–18049.

113 X. e. Jia, Z. Chen, C. Duan, Z. Wang, Q. Yin, F. Huang and Y. Cao, Polythiophene derivatives compatible with both fullerene and non-fullerene acceptors for polymer solar cells, *J. Mater. Chem. C*, 2019, **7**, 314–323.

114 M. Zhang, X. Guo, W. Ma, H. Ade and J. Hou, A polythiophene derivative with superior properties for practical application in polymer solar cells, *Adv. Mater.*, 2014, **26**, 5880–5885.

115 H. Yao, D. Qian, H. Zhang, Y. Qin, B. Xu, Y. Cui, R. Yu, F. Gao and J. Hou, Critical Role of Molecular Electrostatic Potential on Charge Generation in Organic Solar Cells, *Chin. J. Chem.*, 2018, **36**, 491–494.

116 Y. Qin, M. A. Uddin, Y. Chen, B. Jang, K. Zhao, Z. Zheng, R. Yu, T. J. Shin, H. Y. Woo and J. Hou, Highly Efficient Fullerene-Free Polymer Solar Cells Fabricated with Polythiophene Derivative, *Adv. Mater.*, 2016, **28**, 9416–9422.

117 C. Yang, N. Liang, L. Ye, H. Ade, X. Yuan and J. Hou, Enhanced JSC of P3HT-based non-fullerene polymer solar cells by modulating aggregation effect of P3HT in solution state, *Org. Electron.*, 2019, **68**, 15–21.

118 X. Xu, G. Zhang, L. Yu, R. Li and Q. Peng, P3HT-Based Polymer Solar Cells with 8.25% Efficiency Enabled by a Matched Molecular Acceptor and Smart Green-Solvent Processing Technology, *Adv. Mater.*, 2019, **31**, 1906045.

119 Q. Liang, X. Jiao, Y. Yan, Z. Xie, G. Lu, J. Liu and Y. Han, Separating Crystallization Process of P3HT and O-IDTBR to Construct Highly Crystalline Interpenetrating Network with Optimized Vertical Phase Separation, *Adv. Funct. Mater.*, 2019, **29**, 1807591.

120 M. T. Dang, L. Hirsch, G. Wantz and J. D. Wuest, Controlling the morphology and performance of bulk heterojunctions in solar cells. Lessons learned from the benchmark poly(3-hexylthiophene):[6,6]-phenyl-C61-butyric acid methyl ester system, *Chem. Rev.*, 2013, **113**, 3734–3765.